

RADIO OBSERVATIONS OF A SAMPLE OF BROAD-LINED TYPE IC SUPERNOVAE DISCOVERED BY PTF/IPTF: A SEARCH FOR RELATIVISTIC EXPLOSIONS

A. CORSI¹, A. GAL-YAM², S. R. KULKARNI³, D. A. FRAIL⁴, P. A. MAZZALI^{5,6}, S. B. CENKO⁷, M. M. KASLIWAL³, Y. CAO³,
A. HORESH², N. PALLIYAGURU¹, D. A. PERLEY⁸, R. R. LAHER⁹, F. TADDIA¹⁰, G. LELOUDAS^{2,8}, K. MAGUIRE¹¹,
P. E. NUGENT^{12,13}, J. SOLLERMAN¹⁰, M. SULLIVAN¹⁴

December 8, 2024

ABSTRACT

Long duration γ -ray bursts are thought to be a rare subclass of stripped-envelope core-collapse supernovae that launch collimated relativistic outflows (jets). All γ -ray-burst-associated supernovae are spectroscopically of Type Ic with broad lines, but the fraction of broad-lined Type Ic supernovae harboring low-luminosity γ -ray-bursts remains largely unconstrained. Some supernovae should be accompanied by off-axis γ -ray burst jets that remain invisible initially, but then emerge as strong radio sources (as the jets decelerate). However, this critical prediction of the jet model for γ -ray bursts has yet to be verified observationally. Here, we present K. G. Jansky Very Large Array radio observations of 15 broad-lined supernovae of Type Ic discovered by the Palomar Transient Factory in an untargeted manner. Most of the supernovae in our sample exclude radio emission observationally similar to that of the radio-loud, relativistic SN 1998bw. We thus constrain the fraction of 1998bw-like broad-lined Type Ic supernovae to be $\lesssim 14\%$. Most of the events in our sample also exclude off-axis jets similar to GRB 031203 and GRB 030329, but we cannot rule out off-axis γ -ray-bursts expanding in a low-density wind environment. Three supernovae show late-time radio emission compatible with average speeds $\gtrsim 0.3c$, on the dividing line between relativistic and “ordinary” supernovae. Based on these detections, we estimate that $\lesssim 45\%$ of the broad-lined Type Ic supernovae in our sample may harbor off-axis γ -ray-bursts expanding in media with densities in the range probed by this study.

Subject headings: gamma-ray burst: general — radiation mechanisms: non-thermal — supernovae: general — supernovae: individual (PTF10bzf; PTF10qts; PTF10xem; PTF10aavz; PTF11cmh; PTF11img; PTF11lbm; PTF11qcj; PTF12as; iPTF13u; iPTF13alq/SN 2013bn; iPTF13ebw; iPTF14dby; iPTF14gaq; iPTF15dld)

1. INTRODUCTION

Long-duration ($T_\gamma \gtrsim 2$ s) γ -ray bursts (GRBs) are extremely energetic explosions (typically, $\approx 10^{52}$ erg released in ≈ 10 s, also referred to as collapsars) marking

the deaths of massive stars (Galama et al. 1998; Woosley & Bloom 2006). According to the popular fireball model (Piran 2004; Mészáros 2006), the explosion launches relativistic jets in which magnetic fields are amplified and particles accelerated (Rhoads 1999). Observers located within the initial jets’ opening angle ($\theta_j \gtrsim \theta_{obs}$; “on-axis” observers) see an intense flash of γ -rays. Subsequent emission from the decelerating jets produces a (slowly) decaying broad-band afterglow. If the fireball model is correct, then off-axis GRBs should exist and be $\approx 2/\theta_j^2$ times more common than the ones we see in γ -rays (Granot et al. 2002). While γ -ray emission from off-axis GRBs cannot be observed, their longer-wavelength afterglow emission is expected to become observable at later times, once the jet decelerates and starts spreading (Nakar et al. 2002).

Off-axis GRBs have not been discovered so far, but in the light of the well-established connection between long-duration GRBs and core-collapse supernovae (SNe) of spectral type Ic with broad-lines (BL-Ic; Woosley & Bloom 2006), a natural way to search for off-axis events is to observe this type of SNe and wait for the decelerating jet to emerge. While the SN optical emission traces the slower explosion debris ($v \approx 0.03 - 0.1c$), synchrotron emission from the fastest ejecta peaks in the radio band. There can be two major sources of radio emission associated with GRB-SNe,

(i): the SN shock, whose radio emission is brighter and earlier-peaking the faster the SN ejecta,

¹Department of Physics, Texas Tech University, Box 41051, Lubbock, TX 79409-1051, USA. E-mail: alessandra.corsi@ttu.edu

²Benozio Center for Astrophysics, Weizmann Institute of Science, 76100 Rehovot, Israel.

³Division of Physics, Mathematics, and Astronomy, California Institute of Technology, Pasadena, CA 91125, USA.

⁴National Radio Astronomy Observatory, P.O. Box O, Socorro, NM 87801, USA

⁵Astrophysics Research Institute, Liverpool John Moores University, Liverpool L3 5RF, UK.

⁶Max-Planck Institut für Astrophysik, Karl-Schwarzschildstr. 1, D-85748 Garching, Germany.

⁷NASA Goddard Space Flight Center, Code 685, Greenbelt, MD 20771, USA.

⁸Dark Cosmology Centre, Niels Bohr Institute, University of Copenhagen, Juliane Maries Vej 30, 2100 Copenhagen, Denmark.

⁹Spitzer Science Center, California Institute of Technology, M/S 314-6, Pasadena, CA 91125, USA

¹⁰Department of Astronomy, The Oskar Klein Center, Stockholm University, AlbaNova, 10691 Stockholm, Sweden.

¹¹Astrophysics Research Centre, School of Mathematics and Physics, Queen’s University Belfast, Belfast BT7 1NN, UK

¹²Department of Astronomy, University of California, Berkeley, CA 94720-3411, USA.

¹³Lawrence Berkeley National Laboratory, 1 Cyclotron Road, MS 50B-4206, Berkeley, CA 94720, USA

¹⁴Department of Physics and Astronomy, University of Southampton, Southampton, SO17 1SX, UK.

with expected luminosity and peak time of $\approx 10^{29}$ erg cm $^{-2}$ s $^{-1}$ Hz $^{-1}$ and $\approx 10 - 30$ d since explosion, respectively, for relativistic events like SN 1998bw (Galama et al. 1998; Kulkarni et al. 1998; Berger et al. 2003a);

- (ii): the GRB jet which, if off-axis, would be observed only when the SN ejecta decelerate to mildly or sub-relativistic speeds, thus producing a delayed and nearly-isotropized radio emission.

Radio is indeed the best wavelength range for identifying relativistic events such as SN 1998bw, and/or off-axis GRBs (Granot & Loeb 2003; Paczynski 2001). In the past, hundreds of SNe Ib/c have been targeted with the Karl G. Jansky Very Large Array (VLA; Berger et al. 2003a; Soderberg et al. 2006b; Bietenholz et al. 2014) and the fraction of SNe Ib/c associated with GRBs has been constrained to $\lesssim 1 - 3\%$. However, only a very small fraction of the Ic SNe targeted by these past studies were broad-lined, the only type of SNe observationally linked to GRBs. Moreover, many of these SNe Ib/c were located in large, massive, and metal-rich hosts, while GRBs are rarely seen in such galaxies (e.g., Modjaz et al. 2008; Levesque et al. 2010; Hjorth et al. 2012; Graham & Fruchter 2013; Perley et al. 2013; Xu et al. 2013; Kelly et al. 2014; Krühler et al. 2015; Perley et al. 2015). Thus, the fraction of purely BL-Ic SNe harboring relativistic jets remained, observationally, largely unconstrained.

Here, we present a sample of 15 SNe discovered by the Palomar Transient Factory and/or intermediate Palomar Transient Factory (PTF/iPTF, hereafter we use PTF for simplicity; Law et al. 2009; Rau et al. 2009), optimized to search for off-axis GRBs, namely, a sample of BL-Ics selected blindly in random galaxies (mostly dwarfs). While all (long-soft) GRBs may be accompanied by BL-Ic SNe, not all of these SNe make GRBs (e.g., Ofek et al. 2007; Soderberg et al. 2010; Milisavljevic et al. 2015). Why should some stars follow a different path to death, ending their lives as collapsars rather than as “ordinary” SNe, is still a mystery. This study aims at providing additional clues to help gain deeper insight into the nature of collapsar events.

After collecting photometric data (Section 2.1) and classifying the SNe in our sample as belonging to the family of BL-Ic SNe (Section 2.2), we performed X-ray follow-up observations for some of the events (Section 2.3) in search for X-ray signatures (not accompanied by γ -rays) from GRBs observed slightly off-axis (and/or “dirty” fireballs; Section 3). We performed cm-wavelength follow-up observations of all the SNe in our sample with the VLA (Section 2.4), in search for SN 1998bw-like radio emission (point (i) above) and/or later-time signatures of off-axis jets (point (ii) above). Our sample greatly enlarges the sample of radio-monitored BL-Ic SNe published over the last ≈ 10 years (Berger et al. 2003a; Soderberg et al. 2006b; Ghirlanda et al. 2013; Bietenholz et al. 2014), and our observational strategy allows us to probe a portion of the radio luminosity-time since explosion phase space that was left largely unexplored by previous studies (Section 4). We constrain the portion of the explosion energy-wind density parameter space that is excluded under the hypothesis that GRB jets significantly off-axis ($\theta_j \approx 90$ deg)

are associated with the SNe in our sample (Section 5), and set an upper-limit on the fraction of BL-Ic SNe in our sample that show radio emission possibly compatible with off-axis GRBs expanding in media with densities in the range probed by this study (Section 6). Finally, we give our conclusions (Section 7).

Hereafter, we adopt cosmological parameter values of $H_0 = 69.6$ km s $^{-1}$ Mpc $^{-1}$, $\Omega_M = 0.286$, $\Omega_\Lambda = 0.714$ (Wright 2006; Bennett et al. 2014).

2. THE BL-IC SUPERNOVA SAMPLE

2.1. P48 discovery and photometry

R-band (or *g*-band) discoveries (and follow-up) of the SNe in our sample (Table 1) were obtained using the 48-inch Samuel Oschin telescope at the Palomar Observatory (P48), which is routinely used by the PTF/iPTF. Processed images were downloaded from the Infrared Processing and Analysis Center (IPAC) PTF archive (Laher et al. 2014). Photometry was performed relative to the SDSS *r*-band (or *g*-band) magnitudes of stars in the field (York et al. 2000), using our custom pipeline which performs image subtraction followed by point spread function (PSF) photometry on stacks of PTF images extracted from the IPAC archive (Maguire et al. 2012; Ofek et al. 2012, 2013). The flux residuals from individual subtracted images were binned, and then converted to magnitudes. The errors were estimated from the standard deviation of the photometric measurements in each bin.

The *R*-band (or *g*-band) light curves of the SNe in our sample are shown in Fig. 1. PTF10bzf, PTF10qts, and PTF11qej photometry was discussed previously in Corsi et al. (2011), Walker et al. (2014), and Corsi et al. (2014) respectively, so we do not present their photometry here (we refer the reader to these papers). The P48 discovery time (T_{P48}), and the maximum *R*-band (or *g*-band) absolute magnitudes ($M_{R/g}$) as measured by our P48 monitoring and corrected for Galactic extinction (Schlafly & Finkbeiner 2011), are reported in Table 1. Note that our $M_{R/g}$ is different from the SN light curve peak for cases in which the peak emission was not observed by P48. We do not take into account *k*-corrections when measuring $M_{r/g}$, but refer the reader to Prentice et al. 2015 (in prep.) and Taddia et al. 2015 (in prep.) for a discussion of these corrections.

2.2. Spectral classification

After the discovery with P48, we triggered a spectroscopic follow-up campaign¹⁵ of all the SNe in our sample. PTF10bzf, PTF10qts, and PTF11qej spectral properties were previously discussed in Corsi et al. (2011), Walker et al. (2014), and Corsi et al. (2014) respectively, so we do not present their spectral analysis here, but we refer the reader to these papers. For the rest of the SNe in our sample, details of the observations are reported in what follows. In Table 1, we also report the estimated redshifts, and the velocities corresponding to the P-Cygni

¹⁵ All spectra reported in this work will be made public via WISEREP (Yaron & Gal-Yam 2012).

TABLE 1
BL-IC SNE WITH VLA OBSERVATIONS IN OUR SAMPLE. OUR SAMPLE INCLUDES A TOTAL OF 15 SNE, 12 OF WHICH ARE PRESENTED HERE FOR THE FIRST TIME. PTF10BZF, PTF10QTS, AND PTF11QCJ WERE PREVIOUSLY DISCUSSED IN CORSI ET AL. (2011), WALKER ET AL. (2014), AND CORSI ET AL. (2014) RESPECTIVELY.

| PTF name | RA Dec (J2000) (hh:mm:ss deg:mm:ss) | T_{P48}^a (MJD) | z | d_L (Mpc) | $M_{R/g}^b$ [AB] (mag) | v (Si) (km s^{-1}) | Ref. |
|--------------------|--|------------------------|--------|----------------|------------------------------|------------------------------------|----------------------|
| 10bzf | 11:44:02.99 +55:41:27.6 | 55250.504 | 0.0498 | 223 | -18.3 | 2.6×10^4 | Corsi et al. (2011) |
| 10qts | 16:41:37.60 +28:58:21.1 | 55413.260 | 0.0907 | 418 | -19.4 | 1.7×10^4 | Walker et al. (2014) |
| 10xem | 01:47:06.88 +13:56:28.8 | 55470.340 | 0.0567 | 255 | -18.6 | 2.0×10^4 | This paper |
| 10aavz | 11:20:13.36 +03:44:45.2 | 55514.485 | 0.062 | 280 | -19.2 | 1.5×10^4 | This paper |
| 11cmh | 13:10:21.74 +37:52:59.6 | 55673.336 | 0.1055 | 491 | -18.6 | 1.6×10^4 | This paper |
| 11img | 17:34:36.30 +60:48:50.6 | 55755.408 | 0.158 | 761 | -19.6 | 1.5×10^4 | This paper |
| 11lbm | 23:48:03.20 +26:44:33.5 | 55793.259 | 0.039 | 173 | -18.0 | 1.5×10^4 | This paper |
| 11qcj | 13:13:41.51 +47:17:57.0 | 55866.520 ^c | 0.0287 | 124 | -18.0 | 1.2×10^4 | Corsi et al. (2014) |
| 12as | 10:01:34.05 +00:26:58.4 | 55925.298 | 0.033 | 146 | -17.5 | 2.2×10^4 | This paper |
| 13u | 15:58:51.21 +18:13:53.1 | 56324.481 | 0.10 | 463 | -18.9 | 1.0×10^4 | This paper |
| 13alq ^d | 11:48:02.09 +54:34:33.2 | 56394.359 | 0.054 | 242 | -18.9 | 2.3×10^4 | Drake et al. (2013) |
| 13ebw | 08:17:15.88 +56:34:41.6 | 56621.389 | 0.069 | 313 | -18.2 | 2.3×10^4 | This paper |
| 14dby | 15:17:06.29 +25:21:11.4 | 56832.238 | 0.074 | 337 | -17.9 | 1.4×10^4 | This paper |
| 14gaq | 21:32:54.08 +17:44:35.6 | 56924.213 | 0.0826 | 378 | -18.0 | 1.9×10^4 | This paper |
| 15dld ^e | 00:58:13.28 -03:39:50.3 | 57318.322 | 0.047 | 210 | -17.9 | 1.0×10^4 | This paper |

^a Discoveries times (T_{P48}) are from P48 observations in R -band, except for the case of PTF14gaq which was discovered and observed with P48 in g -band.

^b $M_{R/g}$ is the maximum absolute magnitude in the P48 R -band for all of the SNe but PTF14gaq, for which $M_{R/g}$ is measured in the P48 g -band. These magnitudes are corrected for galactic extinction (Schlafly & Finkbeiner 2011).

^c The SN was visible in a previous g -band image taken on 2011 October 23.

^d a.k.a. CSS130415:114802+543439/SN 2013bn: PTF13alq was also discovered by the CRTS (Drake et al. 2013) and classified as a 1998bw-like type Ic SN by the Copernico Telescope in Asiago (Tomasella et al. 2013).

^e PTF15dld/LSQ15bfp was also discovered by the La Silla-QUEST variability survey (Hadjiyska et al. 2012) and classified by the Public ESO Spectroscopic Survey of Transient Objects (PESTO; Smartt et al. 2013).

absorption minimum of the Si II 6355 Å lines, that trace reasonably closely the position of the photosphere (Mazzali et al. 2000, see also Taddia et al. 2015, in prep.).

2.2.1. PTF10xem

On 2010 October 10 UT (≈ 9 d since optical discovery), we observed PTF10xem with the dual-arm Kast spectrograph (Miller & Stone 1993) on the 3 m Shane telescope at Lick Observatory. We used a $2''$ wide slit, a 600/4310 grism on the blue side, and a 300/7500 grating on the red side. Exposure time and air mass were 3600 s and 1.09, respectively. The derived spectrum shows a good match with the Ic/BL-Ic SN 2004aw (e.g., Taubenberger et al. 2006) at an epoch of about 15 d since explosion, and with the BL-Ic SN 2002ap at 6 d since explosion (Fig. 2), so we classify PTF10xem as a BL-Ic SN.

2.2.2. PTF10aavz

On 2010 November 30 UT (≈ 16 d since optical discovery) we observed PTF10aavz using ISIS on the William Herschel Telescope (WHT), with a $1.99''$ wide slit, the R300B grating set at a central wavelength of ≈ 4500 Å on the blue side, and the R158R grating set at a central wavelength of ≈ 7500 Å on the red side. The exposure time was 1800 s, and mean air mass was 1.17. This spectrum of PTF10aavz is most similar to the of the BL-Ic/hyper-energetic and asymmetric SN 2003jd (e.g., Valenti et al. 2008; Mazzali et al. 2005) at an epoch of about 24 d since explosion (Fig. 2).

2.2.3. PTF11cmh

We observed PTF11cmh using ISIS on the WHT on 2011 May 2 UT (≈ 10 d since optical discovery), with a $1.02''$ wide slit, the R300B grating set at a central wavelength of ≈ 4500 Å on the blue side, and the R158R grating set at a central wavelength of ≈ 7500 Å on the red side. For both the blue and red side observations, the exposure time was 900 s and the mean air mass was 1.01. The derived spectrum shows a good match with the Ic/BL-Ic SN 2004aw (e.g., Taubenberger et al. 2006) at an epoch of about 15 d since explosion, and with the BL-Ic SN 2002ap at 6 d since explosion (Fig. 2), so we classify PTF11cmh as a BL-Ic SN.

2.2.4. PTF11img

We observed PTF11img on 2011 August 2 UT (≈ 20 d since optical discovery), using the Low Resolution Imaging Spectrometer (LRIS; Oke et al. 1995) mounted on the Keck-I 10 m telescope. The spectrum was taken using a $1''$ wide slit, with the 400/8500 grating set at a central wavelength of ≈ 7800 Å on the red side, and the 600/4000 grism on the blue side. For both sides, the exposure time and airmass were 600 s and 1.46, respectively. The derived spectrum shows a good match with both the BL-Ic SN 2002ap (e.g., Gal-Yam et al. 2002; Mazzali et al. 2002) at 13 d since explosion, and the type Ic hypernova SN 1997ef (e.g., Iwamoto et al. 1998) at 35 d since explosion (Fig. 2). We thus classify PTF11img as a BL-Ic SN.

2.2.5. PTF11lbm

We observed PTF11lbm using ISIS on the WHT on 2011 August 31 UT (≈ 11 d since optical discovery), with

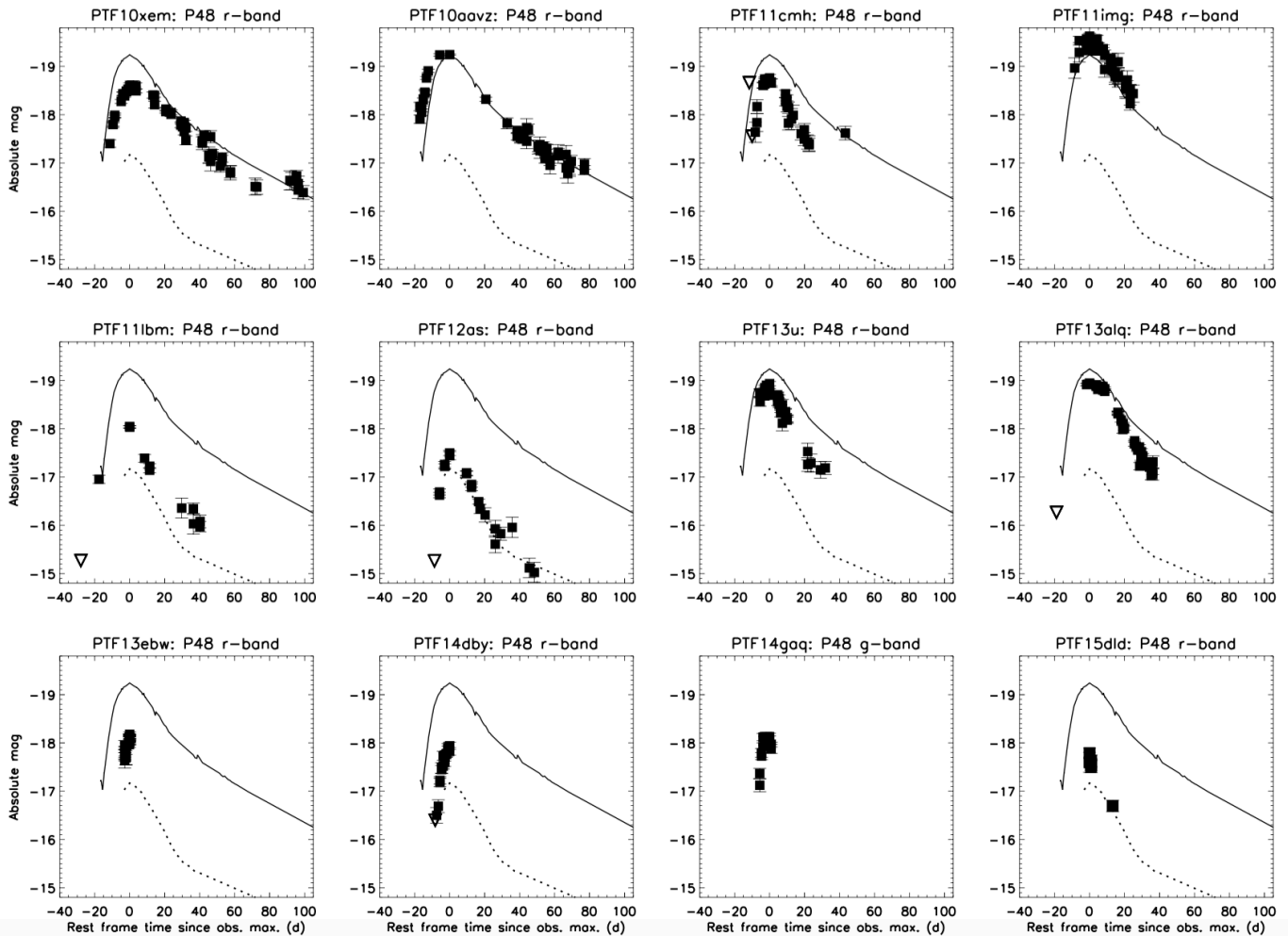


FIG. 1.— The P48 R - or g -band light curves (corrected for Galactic extinction) of the BL-Ic SNe in our sample. PTF names are reported in the title of each panel. For comparison, we also show the r -band light curve of the GRB-associated BL-Ic SN 1998bw (solid line; Clocchiatti et al. 2011), and of the “ordinary” BL-Ic SN 2002ap (dotted line; Pandey et al. 2003). Epochs on the x-axis are measured since the time of maximum emission as observed by P48 (and corrected for redshift effects). Note that the time of maximum as observed by P48 is different from the SN light curve peak time for cases in which the peak emission was not observed by P48.

a $1.02''$ wide slit, the R300B grating set at a central wavelength of $\approx 4500\text{\AA}$ on the blue side; the R158R grating set at a central wavelength of $\approx 7500\text{\AA}$ on the red side. For both the blue and red side observations, the exposure time was 900 s. The mean air mass was about 1.01. The derived spectrum shows a good match with both the BL-Ic SN 2002ap (e.g., Gal-Yam et al. 2002; Mazzali et al. 2002) at 6 d since explosion, and the type Ic hypernova SN 1997ef (e.g., Iwamoto et al. 1998) at 35 d since explosion (Fig. 2). We thus classify PTF11lbn as a BL-Ic SN.

2.2.6. PTF12as

We observed PTF12as on 2012 January 2 UT (≈ 2 d since optical discovery), using the Dual Imaging spectrograph (DIS) mounted on the 3.5 m telescope at the Apache Point Observatory. The spectrum was taken using a $1.5''$ wide slit, with a B400/R300 grating setup. The exposure time and airmass were 1000 s and 1.50, respec-

tively. The derived spectrum shows a good match with the GRB-associated BL-Ic SN 2002ap (e.g., Mazzali et al. 2002; Gal-Yam et al. 2002) at 6 d since explosion (Fig. 2).

2.2.7. PTF13u

On 2013 February 18 UT (≈ 17 d since optical discovery) we observed PTF13u with the Double Beam Spectrograph (DBSP; Oke & Gunn 1982) on the Palomar 200-inch telescope (P200). We used the 316/7500 and 600/4000 gratings for red and blue camera respectively, with a D55 dichroic, resulting in a spectral coverage of $\approx (3500 - 9500)\text{\AA}$. Exposure times and air mass were of 590 s and 1.06, respectively. This spectrum of PTF13u matches that of the BL-Ic/hyper-energetic and asymmetric SN 2003jd (e.g., Valenti et al. 2008; Mazzali et al. 2005) at ≈ 29 d since explosion (Fig. 2).

2.2.8. PTF13alq

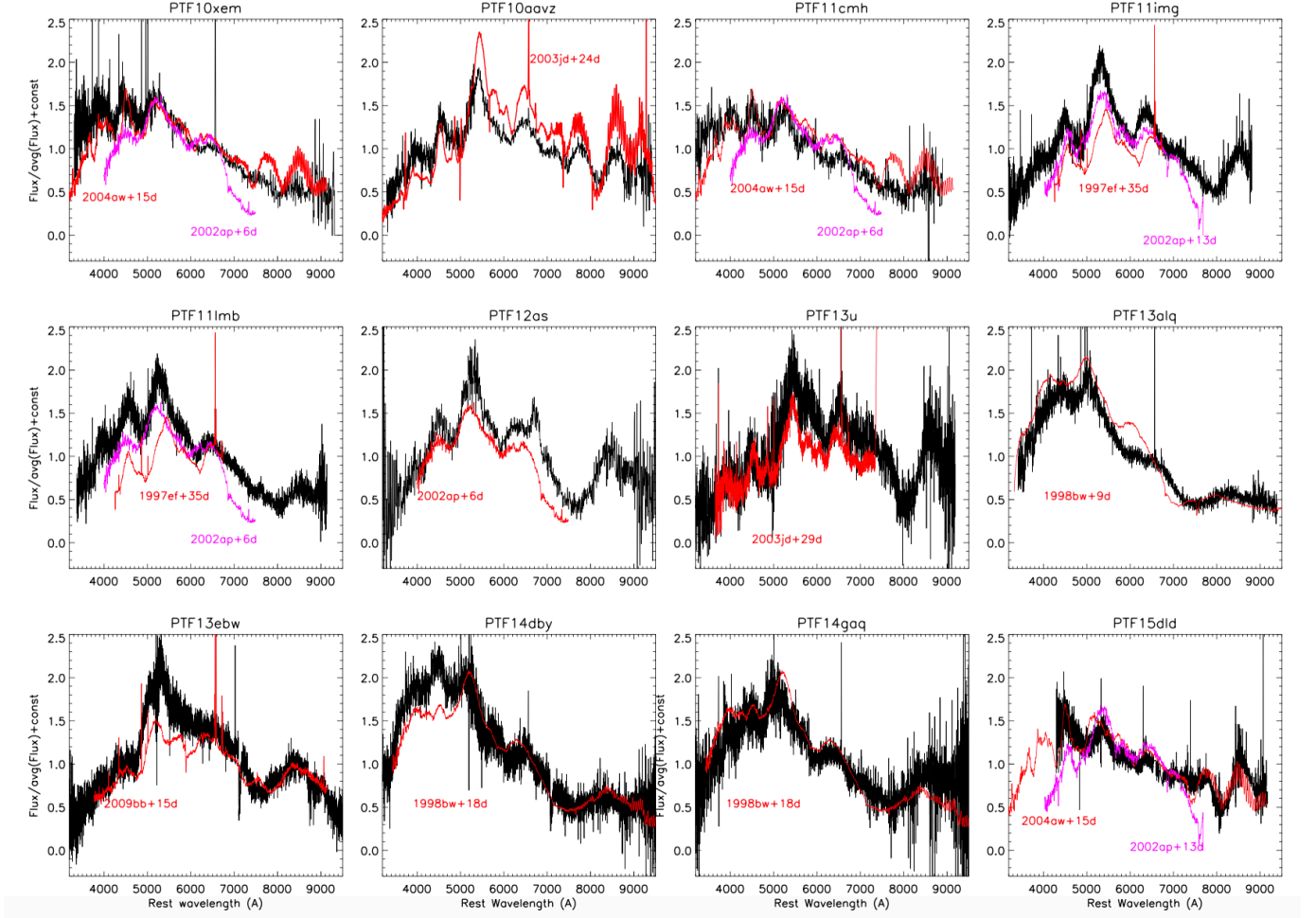


FIG. 2.— Spectra of the SNe BL-Ic in our sample (black) compared to the spectra of the hypernova SN 1997ef (Iwamoto et al. 1998; Branch 1999, epoch calculated since 1997 November 15), of the GRB-associated BL-Ic SN 1998bw (epoch calculated since 1998 April 25; Patat et al. 2001), of the BL-Ic SN 2002ap (epoch calculated since 2002 January 28; Gal-Yam et al. 2002; Mazzali et al. 2002), of the BL-Ic/hyper-energetic and asymmetric SN 2003jd (epoch calculated since 2003 October 21; Valenti et al. 2008; Mazzali et al. 2005; Soderberg et al. 2006b), of the Ic/BL-Ic SN 2004aw (epoch calculated assuming an explosion date of ≈ 15 d before maximum; Taubenberger et al. 2006), and of the relativistic BL-Ic SN 2009bb (yellow - epoch calculated since 2009 March 19; Soderberg et al. 2010; Pignata et al. 2011). (See the electronic version of this paper for colors.)

On 2013 April 13 UT (≈ 1 d since optical discovery) we observed PTF13alq with the DBSP (Oke & Gunn 1982) on P200. We used the 316/7500 and 600/4000 gratings for red and blue camera respectively, with a D55 dichroic, resulting in a spectral coverage of $\approx (3500 - 9500)$ Å. Exposure times and air mass were of 300 s and 1.1, respectively. The derived spectrum shows a good match with the GRB-associated BL-Ic SN 1998bw (e.g., Patat et al. 2001) at 9 d since explosion (Fig. 2).

2.2.9. PTF13ebw

We observed PTF13ebw on 2013 December 4 UT (≈ 9 d since optical discovery), using LRIS mounted on the Keck-I 10 m telescope. The spectrum was taken using a 1'' wide slit, with the 400/8500 grating set at a central wavelength of ≈ 7800 Å on the red side, and the 600/4000 grism on the blue side. The exposure time and airmass were 500 s and 1.36, respectively. The derived spectrum shows a good match with the relativistic BL-Ic

SN 2009bb (Soderberg et al. 2010) at 15 d since explosion (Fig. 2).

2.2.10. PTF14dby

On 2014 June 29 (≈ 5 d since optical discovery), we observed PTF14dby with LRIS mounted on the Keck-I 10 m telescope. The spectrum was taken using a 1'' wide slit, with the 400/8500 grating set at a central wavelength of ≈ 7800 Å on the red side, and the 400/3400 grism on the blue side. The exposure time and airmass were 300 s and 1.19, respectively. This spectrum of PTF14dby reveals a good match with the GRB-associated BL-Ic SN 1998bw (e.g., Patat et al. 2001) at ≈ 18 d since explosion (Fig. 2).

2.2.11. PTF14gaq

We observed PTF14gaq on 2014 October 1 UT (≈ 7 d since optical discovery) with the DBSP on P200. We used the 316/7500 and 600/4000 gratings for the red and

blue camera respectively, with a D55 dichroic, resulting in a spectral coverage of $\approx (3500 - 9500)$ Å. Exposure times and air mass were of 600 s and 1.05, respectively. This spectrum of PTF14gaq shows a good match with the GRB-associated SN1998bw (e.g., Patat et al. 2001) at ≈ 18 d since explosion (Fig. 2).

2.2.12. PTF15dld

We observed PTF15dld on 2015 November 7 UT (≈ 15 d since the P48 optical discovery) with the Deep Extragalactic Imaging Multi-Object Spectrograph (DEIMOS) mounted on the Keck-II 10 m telescope. The spectrum was taken using the 600ZD grating and GG455 filter. The exposure time and airmass were 600 s and 1.11, respectively. The derived spectrum shows a good match with both the BL-Ic SN2002ap (e.g., Gal-Yam et al. 2002; Mazzali et al. 2002) at 13 d since explosion, and with the Ic/BL-Ic SN2004aw (e.g., Taubenberger et al. 2006) at an epoch of about 15 d since explosion (Fig. 2).

2.3. *Swift*/XRT follow-up and data reduction

None of the BL-Ic SNe in our sample was found to be spatially coincident with any of the well-localized GRB in the *Swift* (Gehrels et al. 2004) catalog. For some of the events, we triggered *Swift*/XRT (Burrows et al. 2005) follow-up observations via our approved Target of Opportunity Programs¹⁶ in order to further exclude the presence of a GRB X-ray afterglow with no associated γ -rays (as would be the case for a GRB jet observed slightly off-axis, or for a so-called “dirty” fireball; see e.g. Rhoads 2003).

We downloaded the *Swift*-XRT data from the archive¹⁷. None of the SNe in our sample yielded a detection with *Swift*/XRT, so we calculated 3σ upper-limits on the 0.3-10.0 keV count rate using standard analysis procedures. The upper-limits are reported in Table 2, where we have converted the 0.3-10 keV XRT count rates into fluxes assuming a photon index of $\Gamma_X = 2$ and correcting for Galactic absorption.

X-ray observations of PTF11qcj obtained with *Swift*/XRT and *Chandra*/ACIS (Garmire et al. 2003) were previously presented in Corsi et al. (2014). We include some of these observations (the most significant *Chandra*/ACIS detection and the deepest *Swift*/XRT upper-limit) in Table 2 for completeness.

2.4. VLA follow-up observations and data reduction

We observed all of the SNe in our sample, along with the necessary calibrators, with the VLA¹⁸ (Perley et al. 2009) under our Target of Opportunity programs¹⁹. VLA data were reduced and imaged using the Common Astronomy Software Applications (CASA) package.

¹⁶ Program IDs 1013248 and 1114155 (PI: Corsi).

¹⁷ See <http://heasarc.gsfc.nasa.gov/cgi-bin/W3Browse/swift.pl>.

¹⁸ The National Radio Astronomy Observatory is a facility of the National Science Foundation operated under cooperative agreement by Associated Universities, Inc.; <http://www.nrao.edu/index.php/about/facilities/vlaevla>

¹⁹ VLA/11A-227; VLA/11B-034; VLA/12B-247; VLA/14A-434; VLA/15A-314; PI: A. Corsi.

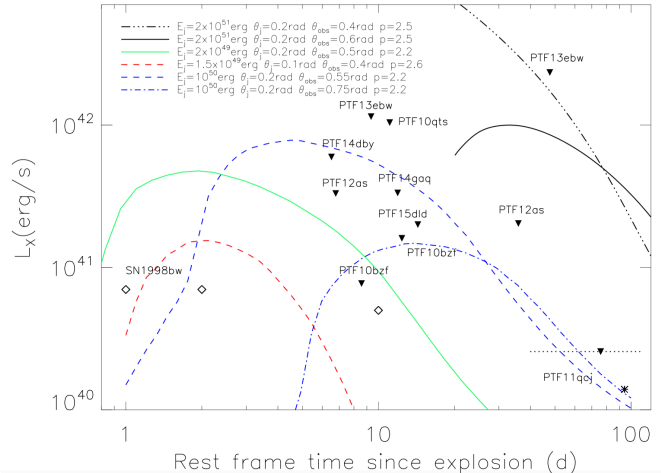


FIG. 3.— *Swift*/XRT upper-limits on some of the BL-Ic SNe in our sample (downward pointing triangles) compared with the X-ray emission from GRB 980425 (diamonds) and with the X-ray emission expected from off-axis GRB models by van Eerten & MacFadyen (2011); van Eerten et al. (2012). GRB jets opening angles are set to $\theta_j = (0.1 - 0.2)$ rad; the medium is a constant density ISM ($n_{ISM} = 1 - 10 \text{ cm}^{-3}$); observer’s viewing angles are in the range $\theta_{obs} \approx (2 - 4)\theta_j$. The fraction of energy density of the ejecta going into electrons (ϵ_e) and magnetic fields (ϵ_B) are both set to 0.1 in all of the above models. We also plot the most significant *Chandra*/ACIS detection of PTF11qcj (asterisk) and the deepest *Swift*/XRT upper limit (dotted line). As evident from this Figure, the X-ray emission from PTF11qcj is dimmer than most GRB off-axis models and we attribute it to the presence of strong CSM interaction rather than to a GRB X-ray afterglow. Some host galaxy contamination to the measured X-ray flux might also be present. See Corsi et al. (2014) for a complete discussion. (See the electronic version of this paper for colors.)

The VLA flux measurements and/or upper-limits are reported in Table 3. The VLA measurement errors are a combination of the rms map error (which measures the contribution of small unresolved fluctuations in the background emission and random map fluctuations due to receiver noise), and a basic fractional error (here estimated to be $\approx 5\%$) which accounts for inaccuracies of the flux density calibration (Weiler et al. 1986; Ofek et al. 2011). The measurement errors reported in Table 3 for the cases in which we had a detection are obtained by summing in quadrature these two contributions to the flux measurement errors.

3. X-RAY CONSTRAINTS ON ASSOCIATED GRB X-RAY AFTERGLOWS

As mentioned in the previous Section, none of the SNe in our sample are spatially coincident with any well-localized GRB. For a limited number of these SNe, our observations with the *Swift*/XRT allow us to make some comparisons with the X-ray light curve that would be expected from an accompanying GRB 980425-like event, or from a high-luminosity GRB observed slightly off-axis. For the last, we use the numerical model by van Eerten & MacFadyen (2011); van Eerten et al. (2012), which considers a relativistic GRB fireball expanding in a uniform density medium.

As evident from Fig. 3, while *Swift*/XRT upper-limits can exclude X-ray afterglows associated with high-luminosity (high-energy) GRBs observed slightly off-axis

TABLE 2
 3σ X-RAY UPPER-LIMITS OR DETECTIONS FOR SOME OF THE SNE IN OUR SAMPLE.

| PTF name | Date (MJD) | ΔT_X^f (days) | Instrument | Band (keV) | Exp. (ks) | N_H^g (10^{20} cm^{-2}) | Count Rate (10^{-4} s^{-1}) | Flux (unabs) ^h ($10^{-14} \text{ erg cm}^{-2} \text{ s}^{-1}$) | Ref. |
|----------|------------|-----------------------|----------------------|------------|-----------|---------------------------------------|---|---|-------------------------|
| 10bzf | 55259.290 | 9 | <i>Swift</i> -XRT | 0.3-10 | 5.0 | 0.88 | < 3.7 | < 1.3 | Kasliwal & Cenko (2010) |
| " | 55263.303 | 13 | <i>Swift</i> -XRT | 0.3-10 | 5.0 | " | < 7.7 | < 2.7 | Kasliwal & Cenko (2010) |
| 10qts | 55426.126 | 13 | <i>Swift</i> -XRT | 0.3-10 | 4.9 | 2.7 | < 4.2 | < 1.6 | This paper |
| 11qcj | 55920.045 | 78 | <i>Swift</i> -XRT | 0.3-10 | 31.4 | 1.0 | < 4.1 | < 1.4 | Corsi et al. (2014) |
| " | 55939.05 | 97 | <i>Chandra</i> -ACIS | 0.3-8.0 | 9.8 | " | 8.8 ± 3.3^i | 0.76 ± 0.26 | Corsi et al. (2014) |
| 12as | 55932.340 | 7 | <i>Swift</i> -XRT | 0.3-10 | 4.6 | 2.5 | < 33 | < 13 | This paper |
| " | 55962.150 | 37 | <i>Swift</i> -XRT | 0.3-10 | 4.9 | " | < 21 | < 8.0 | This paper |
| 13ebw | 56631.719 | 10 | <i>Swift</i> -XRT | 0.3-10 | 4.8 | 4.6 | < 24 | < 9.8 | This paper |
| " | 56672.486 | 51 | <i>Swift</i> -XRT | 0.3-10 | 2.4 | " | < 48 | < 20 | This paper |
| 14dby | 56839.043 | 7 | <i>Swift</i> -XRT | 0.3-10 | 9.5 | 4.2 | < 11 | < 4.4 | This paper |
| 14gaq | 56936.081 | 12 | <i>Swift</i> -XRT | 0.3-10 | 7.8 | 6.9 | < 14 | < 6.1 | This paper |
| 15dld | 57332.973 | 15 | <i>Swift</i> -XRT | 0.3-10 | 9.9 | 3.2 | < 9.8 | < 3.8 | This paper |

^f Epoch in days since P48 discovery (see Table 1), not corrected for redshift effects.

^g Hydrogen column densities are weighted averages from the Leiden/Argentine/Bonn (LAB) Survey of Galactic H I (Kalberla et al. 2005).

^h The count-rate-to-flux conversion assumes a photon index of $\Gamma_X = 2$.

ⁱ *Chandra* observations of PTF11qcj yielded detections which we attribute to the presence of strong CSM interaction rather than to a GRB X-ray afterglow. Some host galaxy contamination to the measured X-ray flux might also be present. See Corsi et al. (2014) for a complete discussion.

(up to $\theta_{obs} \lesssim (2-3)\theta_j$), X-ray emission as faint as the afterglow of the low-luminosity GRB 980425 cannot be excluded. As we discuss in Section 4, radio data collected with the VLA enable us to exclude 1998bw-like emission for most of the SNe in our sample.

For PTF11qcj, *Chandra* observations yielded a detection and the associated X-ray emission is found to be dimmer than most GRB off-axis model. We attribute this emission to the presence of strong CSM interaction rather than to a GRB X-ray afterglow. Some host galaxy contamination to the measured X-ray flux might also be present. See Corsi et al. (2014) for a complete discussion.

4. CONSTRAINING THE FRACTION OF 1998BW-LIKE EVENTS USING RADIO EMISSION

Here, we aim at observationally constraining the fraction of BL-Ic SNe with radio luminosities comparable to that of the GRB-associated SN 1998bw (Kulkarni et al. 1998) to ultimately constrain the fraction of BL-Ic SNe harboring low-luminosity GRBs. Indeed, most of the GRBs with an associated and spectroscopically confirmed SN are low-luminosity bursts ($E_{\gamma,iso} \lesssim 10^{50}$ ergs), although notable exceptions are GRB 030329 (Stanek et al. 2003) and GRB 130427A (e.g., Melandri et al. 2014; Perley et al. 2014). The fraction of BL-Ic SNe harboring low-luminosity GRBs was left largely unconstrained by previous efforts (Berger et al. 2003a; Soderberg et al. 2006b; Bietenholz et al. 2014) due to the very small number of BL-Ic events with radio follow-up available to the community.

Theoretical studies have indirectly constrained the fraction of BL-Ic SNe harboring low-luminosity GRBs by constraining the local rate of low-luminosity GRBs (via luminosity function fitting) and then comparing this estimated local rate with the rate of BL-Ic SNe collected via optical surveys. Following this approach, Guetta & Della Valle (2007) derived that $\gtrsim 10\%$ of BL-Ic SNe are accompanied by low-luminosity GRBs. This is consistent with the earlier results by Podsiadlowski et al. (2004), who found that the rates of GRBs and BL-Ic SNe are comparable to within the uncertainties, and their ratio likely $\gtrsim 30\%$ (see Table 1 in Podsiadlowski et al. 2004). More

recently, following a statistical approach inspired by the Drake equation, Graham & Schady (2015) estimated that there are 4000 ± 2000 BL-Ic SNe in low-metallicity environments for every (long) GRB aligned in our direction. This number is a composite of the fraction of such SNe which produce GRBs and the fraction that are beamed in our direction, and would imply that $\lesssim 5\%$ of the BL-Ic SNe are associated with a GRB.

With our PTF discoveries, we now have a sample of 15 BL-Ic SNe discovered *independently of a GRB trigger*, with at least one radio follow-up observation on timescales $\lesssim 300$ d since explosion (as measured in the SN rest frame; Figs. 4 and 5). Of these 15 SNe, 12 have been uniquely observed via our VLA programs. Our observations have greatly enlarged the sample of 8 BL-Ic SNe with radio follow-up at $\lesssim 300$ d collected via independent efforts during the last decade (Fig. 4, yellow; Fig. 5, green, yellow, and magenta asterisks; Berger et al. 2003a; Chomiuk & Soderberg 2010; Soderberg et al. 2010; Soderberg & Chomiuk 2011; Drake et al. 2013; Kamble & Soderberg 2013; Salas et al. 2013; Chakraborti et al. 2015; Milisavljevic et al. 2015). We are thus in a position to start constraining the theoretical expectations for the low-luminosity GRB-to-BL-Ic SN ratio using a direct observational signature: the presence (or absence) of 1998bw-like radio emission.

In Figs. 4 and 5, the 5 GHz radio light curve of SN 1998bw is compared with the upper-limits and detections obtained for the SNe in our sample (4.8-6.3 GHz; See Table 3). As evident from Fig. 5, we have 3 SNe (PTF11cmh, PTF11qcj, and PTF14dby) that show bright radio emission, much brighter than the ordinary BL-Ic SN 2002ap and almost at the level of SN 1998bw, but their radio peak occurs $\gtrsim 5\times$ later than for SN 1998bw. Thus, as we explain in the following Section, we consider these SNe as observationally different from SN 1998bw, likely related to events on the dividing line between ordinary SNe and GRBs, although an interpretation as off-axis GRB jets might also be possible. For the remaining 12 SNe in our sample, we detect no radio emission and set upper-limits (Fig. 4, black downward-pointing triangles). For 10 of these 12 SNe (all but

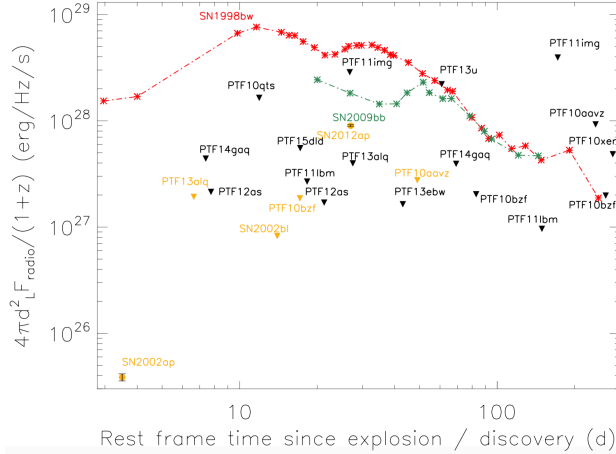


FIG. 4.— Radio (observed central frequencies of $\approx 4.8 - 6.3$ GHz; see Table 3) upper-limits for the BL-Ic SNe in our sample with VLA follow-up observations at $t \lesssim 300$ d since discovery (as measured in the SN rest frame), compared with the light curves of the GRB-SN 1998bw (red asterisks; Kulkarni et al. 1998), of the relativistic BL-Ic SN 2009bb (green asterisks; Soderberg et al. 2010), and of the relativistic SN 2012ap (yellow dot; Chakraborti et al. 2015). Black triangles are our upper-limits. Yellow data points or upper-limits are for BL-Ic SN radio follow-up observations that were not conducted via our programs (Berger et al. 2003a; Chomiuk & Soderberg 2010; Soderberg et al. 2010; Soderberg & Chomiuk 2011; Drake et al. 2013; Kamble & Soderberg 2013; Salas et al. 2013; Chakraborti et al. 2015; Milisavljevic et al. 2015). Radio detections for the PTF sample are plotted in Fig. 5. Late-Time radio observations of BL-Ic SNe performed at $t \gtrsim 300$ d since explosion via other studies (Soderberg et al. 2006b; Bietenholz et al. 2014) are not reported here. (See the electronic version of this paper for colors.)

PTF10xem and PTF13u), we have at least one upper-limit which constrains the radio emission to be dimmer than the emission of SN 1998bw *at a similar epoch*, thus excluding a radio light curve observationally similar to that of the prototype relativistic BL-Ic SN 1998bw. (We note that 8 out of the 12 SNe also exclude radio emission similar to SN 2009bb, a relativistic BL-Ic SN with no associated GRB; Soderberg et al. 2010).

Based on the above results, we conclude that of the 10+3 PTF SNe whose radio observations can set constraints on SN 1998bw-like emission, none of them was in fact like SN 1998bw in the radio i.e., they were all *observationally* different. Adding to this sample the BL-Ic SN 2002ap (Gal-Yam et al. 2002; Mazzali et al. 2002) and SN 2002bl (Armstrong et al. 2002; Berger et al. 2003a), and the CSM-interacting BL-Ic SN 2007bg (Salas et al. 2013), we have a total of 16 BL-Ic SNe for which radio emission observationally similar to SN 1998bw is excluded. Because the 90% confidence Poisson upper-limit on zero SNe compatible with SN 1998bw is 2.3, we conclude that the rate of BL-Ic SNe observationally similar to SN 1998bw $\lesssim 2.3/16 \approx 14\%$. Given that SN 1998bw is the prototype radio SN associated with a low-luminosity GRB, this limit can be considered to ultimately constrain the low-luminosity GRB-to-BL-Ic SN ratio.

5. CONSTRAINING THE FRACTION OF (LARGELY) OFF-AXIS GRBS FROM RADIO NON-DETECTIONS

Low-luminosity GRBs (such as GRB 980425 associated with SN 1998bw) are believed to be intrinsically less en-

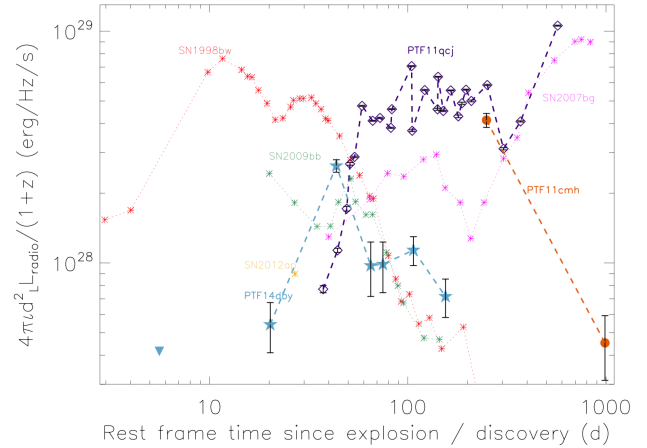


FIG. 5.— BL-Ic SNe in our sample with radio detections: PTF11cmh, orange dots; PTF11qcj, purple diamonds (Corsi et al. 2014); PTF14dby, blue stars. We compare these non-relativistic / CSM-interacting SNe with the light curves of the GRB-SN 1998bw (red asterisks; Kulkarni et al. 1998), of the relativistic BL-Ic SN 2009bb (green asterisks; Soderberg et al. 2010), of the CSM-interacting BL-Ic SN 2007bg (magenta asterisks; Salas et al. 2013), and of the relativistic SN 2012ap (yellow asterisk; Chakraborti et al. 2015). As evident from this comparison, the non-relativistic and CSM-interacting BL-Ic peak at later timescale than the relativistic ones. (See the electronic version of this paper for colors.)

ergetic events (when compared to high-luminosity ones) with jet opening angles $\gtrsim 30$ deg (e.g., Liang et al. 2007). However, the possibility that low-luminosity GRBs are higher-energy events observed off-axis has also been discussed (e.g., Waxman 2004b; Ramirez-Ruiz et al. 2005). Indeed, most (high-luminosity) GRBs are believed to have opening angles of the order of ~ 10 deg (e.g., Frail et al. 2001; Liang et al. 2008; Racusin et al. 2009; Zhang et al. 2015). Here, we aim at answering the question of whether the BL-Ic SNe in our sample that do not show evidence for radio emission observationally similar to that of SN 1998bw (Section 4) could still be accompanied by an off-axis ($\theta_{obs} \approx 90$ deg) GRB afterglow that would become visible in the radio band long past the explosion (at timescales of the order of ~ 1 yr; Levinson et al. 2002; Waxman 2004b; Gal-Yam et al. 2006), when the relativistic fireball enters the sub-relativistic phase and starts spreading, rapidly intersecting the viewer's line of sight while approaching spherical symmetry. Our upper-limits add to the late-time ones that have been collected in the past ($t \gtrsim 500$ d since explosion, not plotted in Figs. 4-5; see Soderberg et al. 2006b; Bietenholz et al. 2014).

To model the late-time radio emission from an off-axis GRB during the non-relativistic phase, we use the analytical model by Waxman (2004b) for a fireball expanding in a wind medium (see e.g. Levinson et al. 2002, for the constant ISM case). In this model the radio luminosity is approximated as:

$$L_r \sim 2.1 \times 10^{29} \left(\frac{\epsilon_e}{0.1}\right) \left(\frac{\epsilon_B}{0.1}\right)^{3/4} \left(\frac{\nu}{10 \text{ GHz}}\right)^{-\frac{(p-1)}{2}} \left(\frac{t}{t_{NR}}\right)^{-3/2} \times A_*^{9/4} E_{51}^{-1/2} \text{ erg s}^{-1} \text{ Hz}^{-1}, \quad (1)$$

where E_{51} is the beaming-corrected ejecta energy; A_*

defines the circumstellar density in terms of the progenitor mass loss-rate \dot{M} and wind velocity v_w such that $A_* = (\dot{M}/10^{-5}M_\odot\text{yr}^{-1})/(v_w/1000\text{ km s}^{-1})$; ϵ_e and ϵ_B are the fraction of ejecta energy density going into electrons and magnetic fields, respectively; and (Waxman 2004b):

$$t_{\text{NR}} \sim 0.3 \left(\frac{E_{51}}{A_*} \right) \text{ yr}, \quad (2)$$

is the time of the non-relativistic transition.

By imposing $t_{\text{NR}} \lesssim t_{\text{obs}}$ and $L_r \gtrsim L_{\text{obs}}$, we can use the VLA upper-limits of the SNe in our sample (Table 3) to exclude the values of (beaming corrected) energy and wind density that would give a radio luminosity above the upper-limits, at the times of our observations. The exclusion regions obtained in this way (and setting $p = 2.2$ and $\epsilon_e = \epsilon_B = 0.1$) are plotted in blue in Fig. 6. We can compare these constraints with the energy and density derived from the broad-band afterglow modeling of the high-luminosity GRB 030329 (for which $\theta_j \approx 5 - 17$ deg, $E_{51} = 0.67$, $A_* \approx 3$; Berger et al. 2003b; Soderberg et al. 2006b) and GRB 130427A (for which $E_{51} \gtrsim 0.5$, $\theta_j \gtrsim 5$ deg, and $0.01 \lesssim A_* \lesssim 0.05$; Perley et al. 2014), and of the low-luminosity GRB 980425 (for which $E_{51} \approx 0.05$ and $A_* \approx 0.04$; Waxman 2004a,b; Soderberg et al. 2006b) and GRB 031203 (for which $E_{51} = 0.017$ and $A_* = 0.6$; Soderberg et al. 2004; Ramirez-Ruiz et al. 2005), all plotted in Fig. 6. From such a comparison we conclude that most of the SNe in our sample exclude GRBs with (beaming corrected) energy and wind density comparable to GRB 030329 and/or GRB 031203, observed largely off-axis and/or during the non-relativistic phase. On the other hand, our upper-limits cannot exclude a GRB as sub-energetic as GRB 980425 observed during its non-relativistic phase, nor an off-axis GRB expanding in a low-density environment such as GRB 130427A.

We finally stress that the shaded regions in Fig. 6 only constrain the portion of the parameter space where $t_{\text{NR}} \lesssim t_{\text{obs}}$. Constraining the portion of the parameter space where $t_{\text{NR}} \gtrsim t_{\text{obs}}$ requires detailed numerical modeling because at $t \lesssim t_{\text{NR}}$, the sideways expansion and the deceleration of the jet depend on the spatial distribution within the jet of the energy density and the Lorentz factor (which are poorly constrained by current observations).

6. VLA DETECTIONS: PTF11CMH AND PTF14DBY

Non-thermal (self-absorbed) synchrotron radiation can be emitted from SN or GRB ejecta during interaction with circumstellar medium (CSM). The temporal and spectral evolution of the synchrotron emission is determined by the dynamics, and by the properties of the ejecta and CSM. While young, non-relativistic SNe expand freely (their ejecta are largely un-decelerated), GRB relativistic blast waves expand and decelerate following the Blandford-McKee solution. At late enough times, both non-relativistic radio SNe and GRBs are expected to approach the non-relativistic adiabatic expansion phase (Sedov-Neumann-Taylor dynamics, see also Section 5). In what follows, we discuss the SNe with radio detections in our sample within these two scenarios (decelerated GRB ejecta and non-relativistic radio SN).

6.1. GRB jets observed off-axis?

Three SNe in our sample, PTF11cmh, PTF11qcj, and PTF14dby, were detected during our radio follow-up with the VLA. Interestingly, two out of these three SNe (PTF11qcj and PTF14dby) are found to be spectroscopically similar to SN 1998bw. Thus, the rate of radio detections for the BL-Ic SNe in our sample *spectroscopically* most similar to SN 1998bw is $\approx 2/4 = 50\%$ (see Fig. 2). As noticed in Section 2.3, the X-ray upper-limit on PTF14dby does *not* exclude the presence of X-ray afterglow emission comparable to that of GRB 980425, however its radio emission appears different from SN 1998bw in the fact that it peaks at later times. Here we address the question of whether the radio emission from PTF11cmh, PTF11qcj, and PTF14dby could be associated with a GRB observed off-axis.

In Figs. 7 and 9 we show a tentative comparison of the observed radio light curves of PTF14dby and PTF11cmh with numerical model light curves of off-axis low-luminosity GRBs expanding in a constant density environment of density n_{ISM} (dashed lines; van Eerten & MacFadyen 2011; van Eerten et al. 2012). We note that numerical models for GRB jets expanding in a wind environment are not currently available to the community (at least not in a format that can allow us to easily compare these models with our observations). Thus, hereafter we limit our discussion to the case of a constant density ISM.

For PTF11cmh (Fig. 7, dashed line), we have set: $\theta_j \approx 11$ deg, observer's angle $\theta_{\text{obs}} \approx 90$ deg, beaming corrected energy $E_{51} \approx 0.1$, $n_{\text{ISM}} = 10\text{ cm}^{-3}$, $\epsilon_B = \epsilon_e \approx 0.1$, and $p \approx 2.2$. These values for the model parameters provide a model light curve in agreement with the (limited) 6 GHz data. We also point out that the limited dataset available for PTF11cmh does leave open the possibility of a mildly-relativistic event (discussed in more detail in the following Section).

For PTF14dby (Fig. 9, dashed line) we have set: $\theta_j \approx 5.7$ deg, observer's angle $\theta_{\text{obs}} \approx 66$ deg, beaming corrected energy $E_{51} \approx 0.01$, $n_{\text{ISM}} = 10\text{ cm}^{-3}$, $\epsilon_B = \epsilon_e \approx 0.1$, and $p \approx 2.4$. While the simplest off-axis GRB model in a constant density ISM does not provide a perfect fit, the model light curves are broadly compatible with the observations of PTF14dby and cannot be securely ruled out. We also note that in the PTF14dby radio light curve there is a hint for a late-time peak (or flattening) reminiscent of SN 1998bw, that may be better fitted using off-axis GRB models expanding in a wind environment, and/or by invoking an energy injection episode similar to what has been proposed by Li & Chevalier (1999) for SN 1998bw.

PTF11qcj is the most difficult to interpret within the simplest off-axis GRB models (see also Corsi et al. 2014): despite there is some amount of controversy in the literature concerning whether the contribution from a GRB counter jet could cause a late-time light curve bump (e.g., Li & Song 2004; Wang et al. 2009; van Eerten & MacFadyen 2011), the clear late-time radio re-brightening observed in PTF11qcj is hard to account for via off-axis model. We note however that this late-time re-brightening requires modifications also to the simplest non-relativistic radio SN model, such as the presence of a denser CSM shell (e.g., Salas et al. 2013).

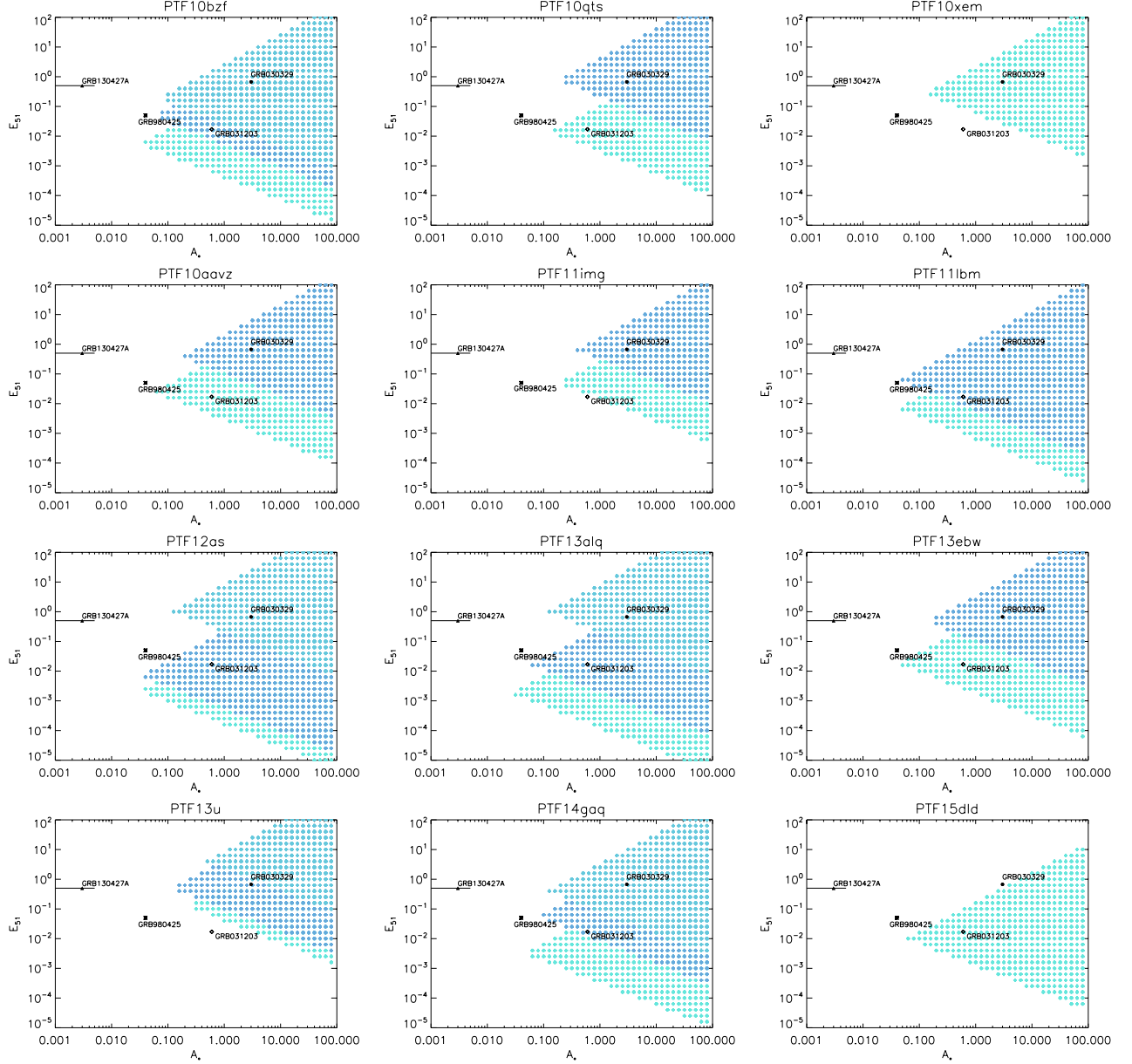


FIG. 6.— Regions of the energy (E_{51}) - density (A_*) parameter space excluded by our VLA upper-limits are shown with different tones of blue. While most of the BL-Ic in our sample exclude off-axis GRBs similar to GRB 030329 and GRB 031203, the VLA upper-limits do not exclude GRBs expanding in a low-density environment such as GRB 130427A observed off-axis (90 deg), or GRBs as sub-energetic as GRB 980425 observed during their non-relativistic phase. (See the electronic version of this paper for colors.)

In summary, a more complete set of numerical GRB off-axis models (especially for the case of a wind environment) is needed. Based on the tentative comparison with available models described in this Section, and on the results described in Section 5, we can attempt to constrain the fraction of BL-Ic SNe in our sample potentially harboring off-axis GRB jets. Indeed, since $\lesssim 3$ BL-Ic SNe in our sample may be associated with off-axis (low-luminosity) GRBs expanding in an ISM with $n_{ISM} \sim 10 \text{ cm}^{-3}$ (or $A_* \sim 4$; compare Eqs. (14) and (15) in Waxman 2004b), we set a 90% Poisson upper-limit of $\lesssim 6.7/15 \approx 45\%$ on the fraction of BL-Ic SNe possibly

harboring off-axis GRBs expanding in media with densities of this order.

6.2. Non-relativistic radio SN emission

In what follows, we model the radio emission observed from PTF11cmh and PTF14dby within the standard radio SN model based on the interaction of non-relativistic ejecta with CSM deposited via a constant mass-loss rate, constant velocity wind (i.e., $\rho_{CSM} = \dot{M}_w / (4\pi v_w r^2)$) from a massive progenitor (Chevalier 1982). We follow the formulation of this standard model given in Soderberg et al. (2005), which replaces the Sedov-Neumann-Taylor dy-

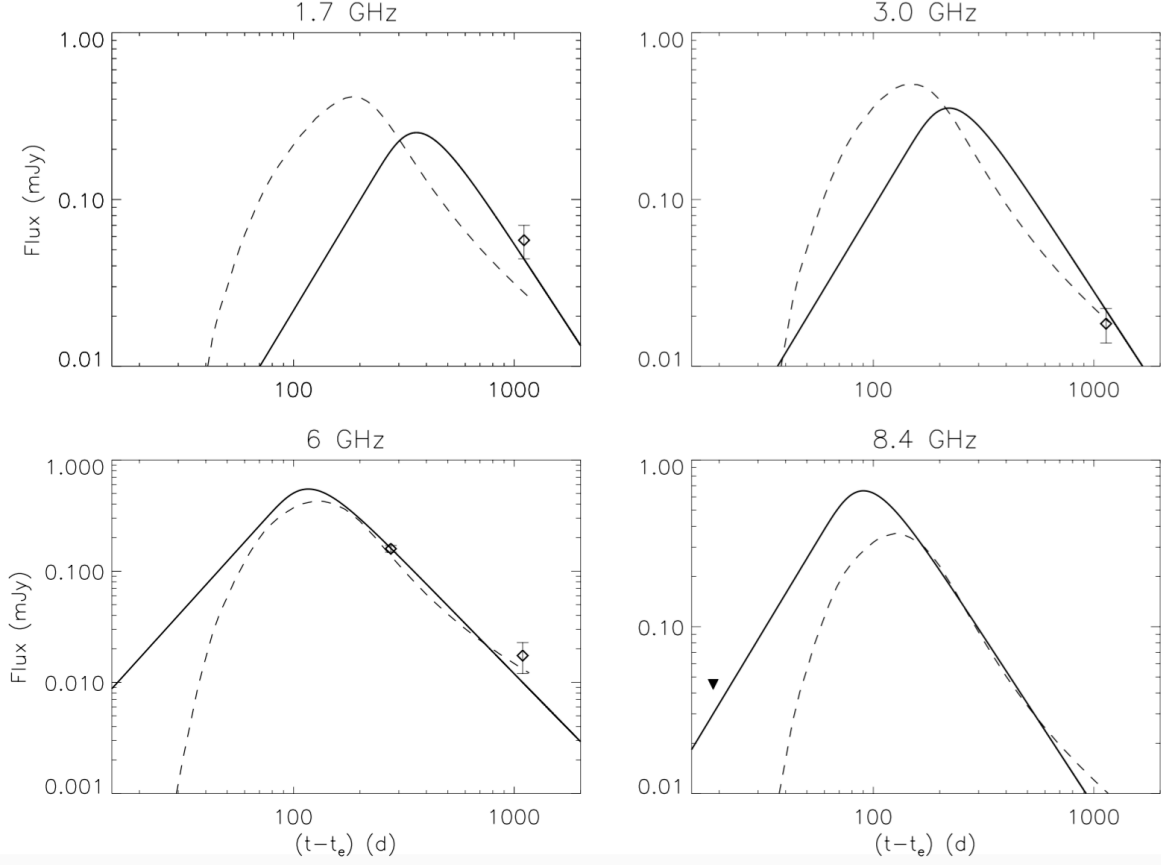


FIG. 7.— Best fit radio light curves of PTF11cmh in the synchrotron self-absorbed radio SN model (solid) and in the off-axis GRB model (dashed), compared with our VLA observations (see Table 3). See text for a discussion of the models and best fit parameters.

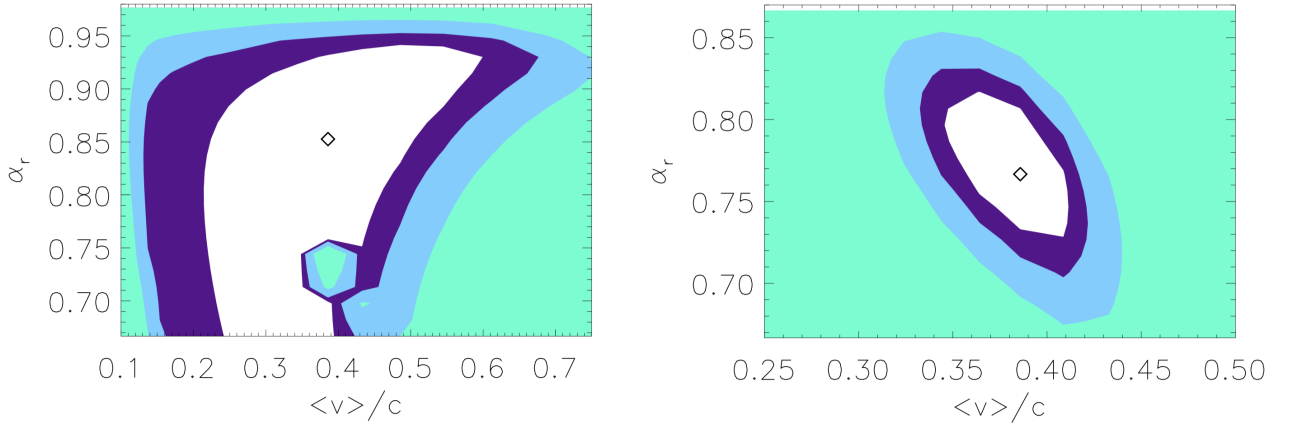


FIG. 8.— PTF11cmh (LEFT) and PTF14dby (RIGHT) best fit results (diamonds) and confidence intervals for the average speed and temporal index of the blastwave radius α_r . We expect $\alpha_r \approx 1$ for an undecelerated explosion, and $\alpha_r \approx 2/3$ for a decelerated explosion in the Sedov-Neumann-Taylor phase (Waxman 2004b). Colors correspond to the following confidence intervals: $\lesssim 68\%$ confidence (white), between 68% and 90% confidence (purple), between 90% and 99% confidence (light blue), and $\gtrsim 99\%$ confidence (aqua green) i.e., contours correspond to $\Delta\chi^2 = 2.3, 4.61, 9.21$ for 2 interesting parameters, respectively. Note that the two χ^2 peaks present at bottom-center of the PTF11cmh plot (aqua green) are portions of the parameter space where the model's physical assumptions break down (i.e., the index p of the electron energy distribution reaches its boundary value of $p = 2$). (See the electronic version of this paper for colors.)

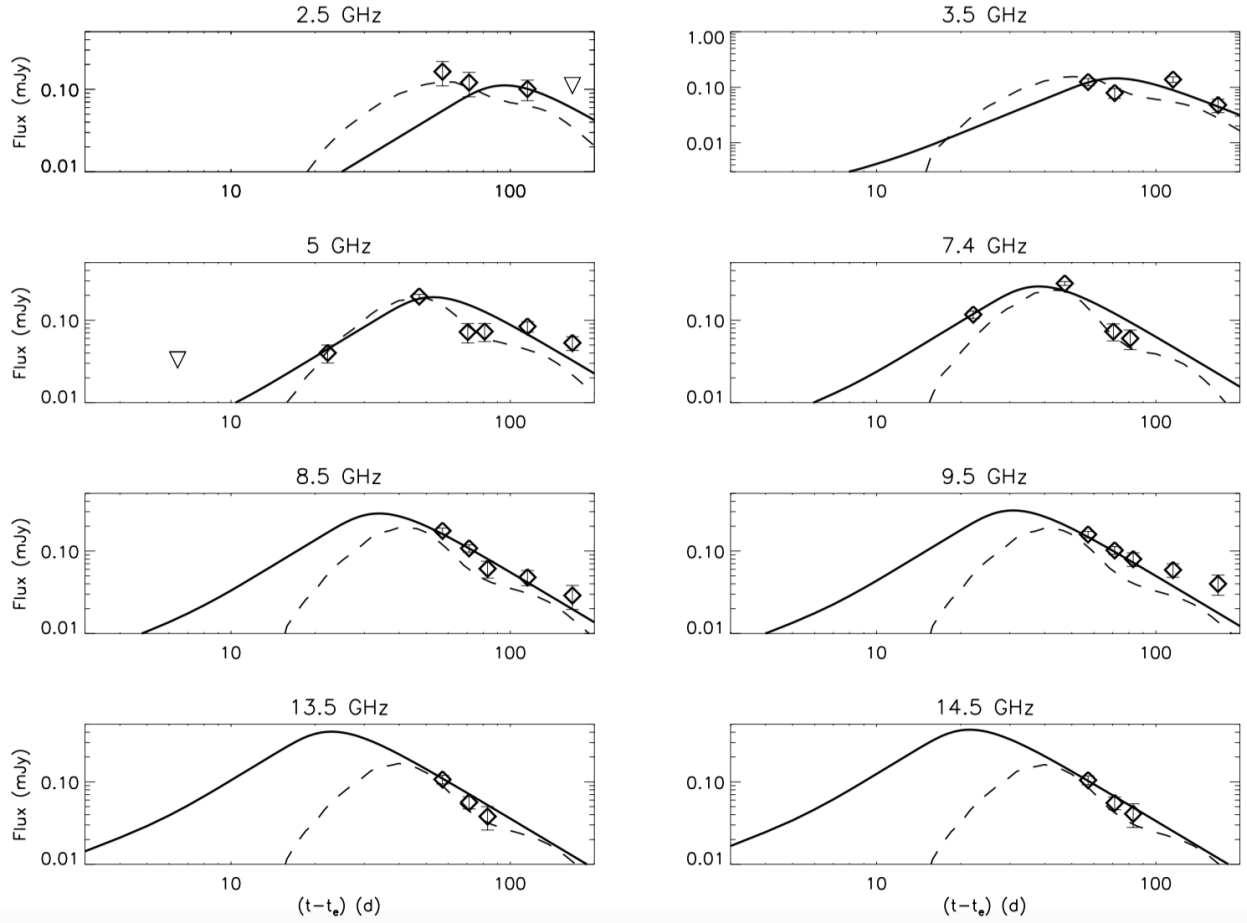


FIG. 9.— Best fit radio light curves of PTF14dbj in the synchrotron self-absorbed radio SN model (solid), and in the off-axis GRB model (dashed), compared with our VLA observations (see Table 3). See text for a discussion of the models and best fit parameters.

namics with a general parametrization of the shock evolution which enables us to model the early SN synchrotron emission (when the ejecta is very close to free expansion), while recovering (in the appropriate time limit) the correct behavior for GRBs transitioning to the sub-relativistic adiabatic expansion phase (Waxman 2004b). We refer the reader to Corsi et al. (2014) for a discussion of PTF11qcj radio emission in the context of the standard radio SN model.

At any time t the observed synchrotron emission originates from a shell of shock-accelerated electrons, with radius r and thickness r/η . The shell expands spherically while following a self-similar evolution in the interaction with a smooth CSM. The electrons are accelerated into a power-law energy distribution $N(\gamma) \propto \gamma^{-p}$, with $\gamma \gtrsim \gamma_m$, and carry a fraction ϵ_e of the energy density of the ejecta. A fraction ϵ_B of the energy density of the ejecta also goes into magnetic fields. The temporal evolution of the radius (r), magnetic field (B), minimum Lorentz factor (γ_m), and of the electrons-to-magnetic field energy ratio (ϵ_e/ϵ_B), is parametrized as follows (Soderberg et al. 2005, 2006a):

$$r = r_0 \left(\frac{t - t_e}{t_0} \right)^{\alpha_r} \quad B = B_0 \left(\frac{t - t_e}{t_0} \right)^{\alpha_B} \quad (3)$$

$$\gamma_m = \gamma_{m,0} \left(\frac{t - t_e}{t_0} \right)^{\alpha_\gamma} \quad \frac{\epsilon_e}{\epsilon_B} = \mathfrak{F}_0 \left(\frac{t - t_e}{t_0} \right)^{\alpha_{\mathfrak{F}}} \quad (4)$$

where t_0 is an arbitrary reference time that we set to day 10 since explosion, and t_e is the explosion time of the SN. In the above equations, $\alpha_r = (n - 3)/(n - s)$ (Chevalier 1982, 1996), where n characterizes the density profile of the outer SN ejecta ($\rho_{\text{SN}} \propto (r/t)^{-n}$), and s characterizes the density profile of the radiating electrons within the shocked CSM ($n_e \propto r^{-s}$).

Following Chevalier (1996), the magnetic energy density ($U_B \propto B^2$) and the relativistic electron energy density ($U_e \propto n_e \gamma_m$) are assumed to be a fixed fraction (i.e., $\alpha_{\mathfrak{F}} = 0$) of the total post-shock energy density ($U \propto n_e \langle v \rangle^2$, where v is the velocity). Making the additional conservative assumption that the energy of the radio emitting material is partitioned equally into accelerating electrons and amplifying magnetic fields ($\epsilon_e = \epsilon_B$, which implies $\mathfrak{F}_0 = 1$) and assuming $s = 2$ (as expected for a wind density profile), we have (Soderberg et al. 2005, 2006a):

$$U_e \propto U \quad \Rightarrow \quad \alpha_\gamma = 2(\alpha_r - 1), \quad (5)$$

and

$$U_B \propto U \quad \Rightarrow \quad \alpha_B = \frac{(2 - s)}{2} \alpha_r - 1 = -1, \quad (6)$$

and, for the flux density from the uniform shell of radiating electrons (Soderberg et al. 2005, 2006a):

$$f_\nu = C_f \left(\frac{t - t_e}{t_0} \right)^{(4\alpha_r + 1)/2} (1 - \exp(-\tau_\nu)) \times \left(\frac{\nu}{1 \text{ GHz}} \right)^{5/2} \times F_3(x) F_2^{-1}(x) \text{ mJy}, \quad (7)$$

where $C_f = C_f(r_0, B_0, p)$ (see Eq. (A.13) in Soderberg

et al. 2005), $x = 2/3(\nu/\nu_m)$, and

$$\nu_m = \gamma_m^2 \frac{eB}{2\pi m_e c} = \gamma_{m,0}^2 \frac{eB_0}{2\pi m_e c} \left(\frac{t - t_e}{t_0} \right)^{2\alpha_\gamma + \alpha_B} = \nu_{m,0} \left(\frac{t - t_e}{t_0} \right)^{4\alpha_r - 5} \quad (8)$$

is the characteristic synchrotron frequency of electrons with Lorentz factor γ_m . Following common practice in radio SNe studies, we set $\nu_{m,0} \approx 1$ GHz (which, in turn, implies that $\gamma_{m,0}$ is a function of B_0 only). In Equation (7), F_2 and F_3 are integrals of the modified Bessel function of order $2/3$ (see Equation (A11) in Soderberg et al. 2005); and

$$\tau_\nu(t) = C_\tau \left(\frac{t - t_e}{t_0} \right)^{(p-2)\alpha_\gamma + (3+p/2)\alpha_B + \alpha_r} \times \left(\frac{\nu}{1 \text{ GHz}} \right)^{-(p+4)/2} F_2(x) = C_\tau \left(\frac{t - t_e}{t_0} \right)^{(2p-1)\alpha_r - (5p/2+1)} \left(\frac{\nu}{1 \text{ GHz}} \right)^{-(p+4)/2} F_2(x) \quad (9)$$

is the optical depth (Soderberg et al. 2005, 2006a), with $C_\tau = C_\tau(r_0, B_0, \gamma_{m,0}, p)$ (see Eq. (A.14) in Soderberg et al. 2005). Thus, as evident from Eqs. 7 and 9, the observed spectral and temporal evolutions of the radio emission ultimately depend on the parameters ($r_0, B_0, t_e, p, \alpha_r, \eta$), which we determine by comparison with the data.

6.2.1. PTF11cmh radio modeling

Our VLA follow-up observations of PTF11cmh started at an epoch of about ≈ 20 d since optical discovery, and were carried out until more than 10^3 d after (Table 3). Our first radio detection of PTF11cmh was more than 100 d since optical discovery.

Modeling our radio observations in the standard synchrotron self-absorbed scenario (Section 6.2) using a χ^2 minimization procedure where we set $t_e = 55673.336$ MJD (see Table 1) and $\eta = 5$, we get $\chi^2 \approx 4$ for 1 d.o.f.²⁰. From the best fit light curves shown in Fig. 7 (solid lines), we also estimate $\nu_p \approx 5$ GHz at ≈ 100 d since explosion, and $L_{p,5 \text{ GHz}} \approx 10^{29} \text{ erg s}^{-1} \text{ Hz}^{-1}$. The last is comparable to the radio spectral luminosity of the GRB-associated SN 1998bw (Kulkarni et al. 1998).

The best-fit values for the model parameters are $p \approx 3.3$, $B_0 \approx 4.6$ G, and a blast-wave radial evolution of $R \approx 1.0 \times 10^{16} [(t - t_e)/10 \text{ d}]^{0.85} \text{ cm}$. The last implies an average ejecta speed of $R/\Delta t \approx 0.39c$, where c is the speed of light. This is $\approx 3 - 4\times$ higher than the average speed of ordinary Ib/c SNe ($\approx 0.1c$), but smaller than relativistic events such as SN 2009bb and SN 1998bw. However, as evident from Fig. 8, because of the limited dataset available for this event, the speed of the radio emitting material is affected by large errors.

Making the conservative assumption that the energy of the radio emitting material is partitioned equally into accelerating electrons and amplifying magnetic fields

²⁰ We do not expect the simplified analytical synchrotron model to provide a perfect fit, and this value of the χ^2 is similar to what obtained in other analyses of radio SN light curves.

($\epsilon_e = \epsilon_B = 0.33$), we derive a minimum energy of $E \approx 6 \times 10^{48} (\epsilon_e/0.33)^{-1} [(t - t_e)/10 \text{ d}]^{0.55}$ erg coupled to the fastest radio-emitting outflow. This energy is at the higher end of the range derived for other radio Ib/c SNe (Margutti et al. 2014).

Finally, the estimated progenitor mass-loss rate is $\dot{M} = 9 \times 10^{-5} (v_w/1000 \text{ km s}^{-1}) M_\odot \text{ yr}^{-1}$, where v_w is the velocity of the stellar wind and where we have assumed a nucleon-to-proton ratio of 2. This mass-loss rate is higher than the typical range derived for low-luminosity GRBs (see e.g. Fig. 6), and more similar to CSM-interacting BL-Ic SNe such as PTF11qcj (Corsi et al. 2014). We thus conclude that PTF11cmh is likely to be a CSM-interacting event similar to PTF 11qcj, although this conclusion has to be taken with the caveat of being derived from a limited dataset.

6.2.2. PTF14dby radio modeling

Our VLA follow-up observations of PTF14dby started at an epoch of about ≈ 6 d since optical discovery, and were carried out until more than 150 d after (Table 3). The first clear ($\gtrsim 4\sigma$) VLA detection of PTF14dby at 5 GHz was obtained about 20 d since optical discovery.

Modeling our radio observations in the standard synchrotron self-absorbed scenario (Section 6.2) using a χ^2 minimization procedure where we set $\eta = 5$, we get $\chi^2 \approx 115$ for 31 d.o.f.. From the best fit light curves shown in Fig. 9 (solid lines) we estimate $\nu_p \approx 7.4$ GHz at ≈ 40 d since explosion, and a spectral peak luminosity of $L_{p,7.4\text{GHz}} \approx 2.7 \times 10^{28} \text{ erg s}^{-1} \text{ Hz}^{-1}$. The last is $\approx 4\times$ smaller than the peak radio luminosity of the GRB-associated SN 1998bw, but comparable to the radio peak luminosity of the engine-drive SN 2009bb (Fig. 5; Soderberg et al. 2010).

The best-fit values for the model parameters are $t_e \approx 56831.8$ MJD (which is consistent with the discovery date reported in Table 1), $p \approx 2.9$, $B_0 \approx 1.6$ G, and a blast-wave radial evolution of $R \approx 9.9 \times 10^{15} [(t - t_e)/10 \text{ d}]^{0.77}$ cm. The last implies an average ejecta speed of $R/\Delta t \approx 0.38 c$. This is $\approx 3 - 4\times$ higher than the average for ordinary Ib/c SNe ($\approx 0.1c$), but smaller than relativistic events such as SN 2009bb and SN 1998bw.

Making the conservative assumption that the energy of the radio emitting material is partitioned equally into accelerating electrons and amplifying magnetic fields ($\epsilon_e = \epsilon_B = 0.33$), we derive a minimum energy of $E \approx 7.9 \times 10^{47} (\epsilon_e/0.33)^{-1} [(t - t_e)/10 \text{ d}]^{0.32}$ erg coupled to the fastest radio-emitting outflow.

Finally, the estimated progenitor mass-loss rate is $\dot{M} = 5.3 \times 10^{-6} (v_w/1000 \text{ km s}^{-1}) M_\odot \text{ yr}^{-1}$ (where again we have assumed a nucleon-to-proton ratio of 2). This mass-loss rate is in agreement with values derived for low-luminosity GRBs (see e.g. Fig. 6), and smaller than the one derived for CSM-interacting BL-Ic SNe such as PTF11qcj ($\dot{M} \approx 10^{-4} (v_w/1000 \text{ km s}^{-1}) M_\odot \text{ yr}^{-1}$; Corsi

et al. 2014). This, together with the fact that the simplest off-axis GRB models (dashed lines in Fig. 9) are in broad agreement with the radio light curve of PTF14dby, calls for a more accurate numerical modeling of this SN which is beyond the scope of this paper, but that we hope will get the attention of the community.

7. SUMMARY AND CONCLUSION

We have presented the P48 photometry, spectral classification, and radio/X-ray follow-up observations of 15 BL-Ic SNe discovered by the PTF/iPTF. Thanks to deep VLA follow-up observations, we are able to exclude the presence of 1998bw-like (or 2009bb-like) radio emission for most of the SNe in our sample. Because radio emission traces the fastest moving ejecta, we conclude that events as relativistic as, and observationally similar to, SN 1998bw are $\lesssim 14\%$ of the BL-Ic population.

Using the X-ray upper-limits collected via our programs, we rule out the presence of off-axis GRB jets observed slightly off-axis for some of the SNe in our sample. We also constrain the energy and density parameters of (largely) off-axis GRBs potentially harbored by the SNe in our sample for which 1998bw-like radio emission was excluded. While we can rule out the presence of GRBs as energetic as GRB 030329 observed at large off-axis angles and expanding in wind mediums with densities $A_* \gtrsim 0.1$, we cannot rule out the presence of off-axis GRBs expanding in a less dense medium, such as the one found around GRB 130427A.

Finally, we presented the detailed radio modeling of two radio-loud BL-Ic, PTF11cmh and PTF14dby, which add to our previous radio detection of PTF11qcj. We constrained the speed of the radio emitting material to be intermediate between that of non-relativistic BL-Ic SNe, and relativistic events such as SN 2009bb. Because we cannot securely rule out off-axis GRB models for these three events, we set an upper-limit of $\lesssim 45\%$ on the fraction of BL-Ic SNe in our sample that could potentially harbor a GRB observed off-axis and expanding in a medium of density $n_{ISM} \sim 10 \text{ cm}^{-3}$. This estimate could be improved by comparing our data with numerical models for off-axis GRBs expanding in a wind medium.

In summary, our results show that the VLA (thanks to its improved sensitivity) working in tandem with surveys like the iPTF, can help us clarify key open questions regarding the GRB-SN connection (such as, what fraction of purely BL-Ic SNe can host low-luminosity GRBs) and enable us to discover more events on the dividing line between ordinary BL-Ic and relativistic GRBs. Over the course of 5 years, we have greatly enlarged the sample of BL-Ic SNe (discovered independently of a GRB trigger) with radio follow-up within one year since discovery. We expect that the Zwicky Transient Factor will be able to boost even further the rate at which we are discovering the rare BL-Ic events (Smith et al. 2014).

REFERENCES

- Armstrong, M., et al. 2002, IAUC, 7845
 Bennett, C. L., Larson, D., Weiland, J. L., & Hinshaw, G. 2014, ApJ, 794, 135
 Berger, E., Kulkarni, S. R., Frail, D. A., & Soderberg, A. M. 2003a, Astrophys. J., 599, 408
 Berger, E., et al. 2003b, Nature, 426, 154
 Bietenholz, M. F., De Colle, F., Granot, J., Bartel, N., & Soderberg, A. M. 2014, MNRAS, 440, 821
 Branch, D. 1999, ArXiv Astrophysics e-prints, astro-ph/9906168
 Burrows, D. N., et al. 2005, Space Sci. Rev., 120, 165
 Chakraborti, S., et al. 2015, ApJ, 805, 187
 Chevalier, R. A. 1982, Astrophys. J., 259, 302

- Chevalier, R. A. 1996, in *Astronomical Society of the Pacific Conference Series*, Vol. 93, *Radio Emission from the Stars and the Sun*, ed. A. R. Taylor & J. M. Paredes, 125
- Chomiuk, L., & Soderberg, A. 2010, *The Astronomer's Telegram*, 2483, 1
- Clocchiatti, A., Suntzeff, N. B., Covarrubias, R., & Candia, P. 2011, *AJ*, 141, 163
- Corsi, A., et al. 2011, *Atrophys. J.*, 741, 76
- Corsi, A., et al. 2014, *ApJ*, 782, 42
- Drake, A. J., et al. 2013, *The Astronomer's Telegram*, 4984, 1
- Frail, D. A., et al. 2001, *ApJ*, 562, L55
- Gal-Yam, A., et al. 2010, *The Astronomer's Telegram*, 2817, 1
- Gal-Yam, A., et al. 2006, *ApJ*, 639, 331
- Gal-Yam, A., Ofek, E. O., & Shemmer, O. 2002, *Mon. Not. Roy. Astr. Soc.*, 332, L73
- Galama, T. J., et al. 1998, *Nature*, 395, 670
- Garmire, G. P., Bautz, M. W., Ford, P. G., Nousek, J. A., & Ricker, G. R., Jr. 2003, in *Society of Photo-Optical Instrumentation Engineers (SPIE) Conference Series*, Vol. 4851, *X-Ray and Gamma-Ray Telescopes and Instruments for Astronomy*, ed. J. E. Truemper & H. D. Tananbaum, 28
- Gehrels, N., et al. 2004, *Astrophys. J.*, 611, 1005
- Ghirlanda, G., et al. 2013, *Mon. Not. Roy. Astr. Soc.*, 428, 1410
- Graham, J. F., & Fruchter, A. S. 2013, *ApJ*, 774, 119
- Graham, J. F., & Schady, P. 2015, *ArXiv e-prints* 1511.01466
- Granot, J., & Loeb, A. 2003, *Astrophys. J. Lett.*, 593, L81
- Granot, J., Panaitescu, A., Kumar, P., & Woosley, S. E. 2002, *Astrophys. J. Lett.*, 570, L61
- Guetta, D., & Della Valle, M. 2007, *ApJL*, 657, L73
- Hadjijska, E., et al. 2012, in *IAU Symposium*, Vol. 285, *IAU Symposium*, ed. E. Griffin, R. Hanisich, & R. Seaman, 324
- Hjorth, J., et al. 2012, *ApJ*, 756, 187
- Iwamoto, K., et al. 1998, *ArXiv Astrophysics e-prints*
- Kalberla, P. M. W., Burton, W. B., Hartmann, D., Arnal, E. M., Bajaja, E., Morras, R., & Pöppel, W. G. L. 2005, *A&A*, 440, 775
- Kamble, A., & Soderberg, A. 2013, *The Astronomer's Telegram*, 4997, 1
- Kasliwal, M. M., & Cenko, S. B. 2010, *The Astronomer's Telegram*, 2471, 1
- Kelly, P. L., Filippenko, A. V., Modjaz, M., & Kocevski, D. 2014, *ApJ*, 789, 23
- Krühler, T., et al. 2015, *A&A*, 581, A125
- Kulkarni, S. R., et al. 1998, *Nature*, 395, 663
- Laher, R. R., et al. 2014, *PASP*, 126, 674
- Law, N. M., et al. 2009, *Pub. of the Astron. Soc. of the Pacific*, 121, 1395
- Levesque, E. M., Kewley, L. J., Berger, E., & Zahid, H. J. 2010, *AJ*, 140, 1557
- Levinson, A., et al. 2002, *Astrophys. J.*, 576, 923
- Li, Z., & Song, L. M. 2004, *ApJ*, 614, L17
- Li, Z.-Y., & Chevalier, R. A. 1999, *ApJ*, 526, 716
- Liang, E., Zhang, B., Virgili, F., & Dai, Z. G. 2007, *ApJ*, 662, 1111
- Liang, E.-W., Racusin, J. L., Zhang, B., Zhang, B.-B., & Burrows, D. N. 2008, *ApJ*, 675, 528
- Maguire, K., et al. 2012, *Mon. Not. Roy. Astr. Soc.*, 426, 2359
- Margutti, R., et al. 2014, *ApJ*, 797, 107
- Mazzali, P. A., et al. 2002, *Astrophys. J. Lett.*, 572, L61
- Mazzali, P. A., Iwamoto, K., & Nomoto, K. 2000, *Astrophys. J.*, 545, 407
- Mazzali, P. A., et al. 2005, *Science*, 308, 1284
- Melandri, A., et al. 2014, *A&A*, 567, A29
- Mészáros, P. 2006, *Reports on Progress in Physics*, 69, 2259
- Milisavljevic, D., et al. 2015, *ApJ*, 799, 51
- Miller, J. S., & Stone, R. 1993, *Lick Ob. Tech. Rep.* 66
- Modjaz, M., et al. 2008, *AJ*, 135, 1136
- Nakar, E., Piran, T., & Granot, J. 2002, *Astrophys. J.*, 579, 699
- Ofek, E. O., et al. 2007, *ApJ*, 662, 1129
- Ofek, E. O., Frail, D. A., Breslauer, B., Kulkarni, S. R., Chandra, P., Gal-Yam, A., Kasliwal, M. M., & Gehrels, N. 2011, *Astrophys. J.*, 740, 65
- Ofek, E. O., et al. 2012, *Pub. of the Astron. Soc. of the Pacific*, 124, 62
- Ofek, E. O., et al. 2013, *Nature*, 494, 65
- Oke, J. B., et al. 1995, *PASP*, 107, 375
- Oke, J. B., & Gunn, J. E. 1982, *Pub. of the Astron. Soc. of the Pacific*, 94, 586
- Paczynski, B. 2001, *Acta Astronomica*, 51, 1
- Pandey, S. B., Anupama, G. C., Sagar, R., Bhattacharya, D., Sahu, D. K., & Pandey, J. C. 2003, *MNRAS*, 340, 375
- Patat, F., et al. 2001, *Astrophys. J.*, 555, 900
- Perley, D. A., et al. 2014, *ApJ*, 781, 37
- Perley, D. A., et al. 2015, *ArXiv e-prints* arXiv150402482P
- Perley, D. A., et al. 2013, *ApJ*, 778, 128
- Perley, R., et al. 2009, *IEEE Proceedings*, 97, 1448
- Pignata, G., et al. 2011, *Astrophys. J.*, 728, 14
- Piran, T. 2004, *Reviews of Modern Physics*, 76, 1143
- Podsiadlowski, P., Mazzali, P. A., Nomoto, K., Lazzati, D., & Cappellaro, E. 2004, *ApJ*, 607, L17
- Racusin, J. L., et al. 2009, *ApJ*, 698, 43
- Ramirez-Ruiz, E., Granot, J., Kouveliotou, C., Woosley, S. E., Patel, S. K., & Mazzali, P. A. 2005, *ApJ*, 625, L91
- Rau, A., et al. 2009, *Pub. of the Astron. Soc. of the Pacific*, 121, 1334
- Rhoads, J. E. 1999, *Astrophys. J.*, 525, 737
- Rhoads, J. E. 2003, *ApJ*, 591, 1097
- Salas, P., Bauer, F. E., Stockdale, C., & Prieto, J. L. 2013, *Mon. Not. Roy. Astr. Soc.*, 428, 1207
- Schlafly, E. F., & Finkbeiner, D. P. 2011, *Astrophys. J.*, 737, 103
- Smartt, S. J., et al. 2013, *The Messenger*, 154, 50
- Smith, R. M., et al. 2014, in *Society of Photo-Optical Instrumentation Engineers (SPIE) Conference Series*, Vol. 9147, *Society of Photo-Optical Instrumentation Engineers (SPIE) Conference Series*, 79
- Soderberg, A., & Chomiuk, L. 2011, *The Astronomer's Telegram*, 3101, 1
- Soderberg, A. M., et al. 2010, *Nature*, 463, 513
- Soderberg, A. M., Chevalier, R. A., Kulkarni, S. R., & Frail, D. A. 2006a, *Astrophys. J.*, 651, 1005
- Soderberg, A. M., Kulkarni, S. R., Berger, E., Chevalier, R. A., Frail, D. A., Fox, D. B., & Walker, R. C. 2005, *Astrophys. J.*, 621, 908
- Soderberg, A. M., et al. 2004, *Nature*, 430, 648
- Soderberg, A. M., Nakar, E., Berger, E., & Kulkarni, S. R. 2006b, *Astrophys. J.*, 638, 930
- Staneck, K. Z., et al. 2003, *ApJ*, 591, L17
- Taubenberger, S., et al. 2006, *Mon. Not. Roy. Astr. Soc.*, 371, 1459
- Tomasella, L., Benetti, S., Pastorello, A., Cappellaro, E., Turatto, M., & Ochner, P. 2013, *The Astronomer's Telegram*, 4989, 1
- Valenti, S., et al. 2008, *Mon. Not. Roy. Astr. Soc.*, 383, 1485
- van Eerten, H., van der Horst, A., & MacFadyen, A. 2012, *ApJ*, 749, 44
- van Eerten, H. J., & MacFadyen, A. I. 2011, *Astrophys. J.L.*, 733, L37
- Walker, E. S., et al. 2014, *MNRAS*, 442, 2768
- Wang, X., Huang, Y. F., & Kong, S. W. 2009, *A&A*, 505, 1213
- Waxman, E. 2004a, *ApJ*, 605, L97
- Waxman, E. 2004b, *ApJ*, 602, 886
- Weiler, K. W., Sramek, R. A., Panagia, N., van der Hulst, J. M., & Salvati, M. 1986, *Astrophys. J.*, 301, 790
- Woosley, S. E., & Bloom, J. S. 2006, *Ann. Rev. Astron. Astrophys.*, 44, 507
- Wright, E. L. 2006, *PASP*, 118, 1711
- Xu, D., et al. 2013, *ApJ*, 776, 98
- Yaron, O., & Gal-Yam, A. 2012, *Pub. of the Astron. Soc. of the Pacific*, 124, 668
- York, D. G., et al. 2000, *The Astronomical Journal*, 120, 1579
- Zhang, B.-B., van Eerten, H., Burrows, D. N., Ryan, G. S., Evans, P. A., Racusin, J. L., Troja, E., & MacFadyen, A. 2015, *ApJ*, 806, 15

A.C. acknowledges support from the NSF CAREER award #1455090. A.C. and N.P. acknowledge partial support from NASA/Swift Cycle 10 and 11 GI via grants NNX15AB79G and NNX16AC12G. A.G.-Y.'s team is supported by the EU/FP7 via ERC grant no. 307260, the Quantum Universe I-Core program by the Israeli Committee for planning

and budgeting and the ISF; by Minerva and ISF grants; by the Weizmann-UK “making connections” program; and by Kimmel and ARCHES awards. K.M. acknowledges support from the STFC through an Ernest Rutherford Fellowship. M. S. acknowledges support from the Royal Society and EU/FP7-ERC grant no. 615929. The Karl G. Jansky Very Large Array is operated by NRAO, for the NSF under cooperative agreement by Associated Universities, Inc. W. M. Keck Observatory, is operated as a scientific partnership among the California Institute of Technology, the University of California and the National Aeronautics and Space Administration. The Observatory was made possible by the generous financial support of the W. M. Keck Foundation. The William Herschel Telescope is operated on the island of La Palma by the Isaac Newton Group in the Spanish Observatorio del Roque de los Muchachos of the Instituto de Astrofísica de Canarias. The authors acknowledge the High Performance Computing Center (HPCC) at Texas Tech University at Lubbock (<http://cmsdev.ttu.edu/hpcc>) for providing HPC resources that have contributed to the research results reported within this paper. This research also used resources of the National Energy Research Scientific Computing Center, a DOE Office of Science User Facility supported by the Office of Science of the U.S. Department of Energy under Contract No. DE-AC02-05CH11231.

TABLE 3 VLA observations. For non-detections, the quoted UL are at 3σ (where σ is the image rms) unless otherwise stated.

| PTF Name | $T_{\text{VLA}}^{\text{j}}$ (MJD) | $\Delta T_{\text{VLA}}^{\text{k}}$ (d) | Conf. | ν (GHz) | BW (MHz) | Flux (μJy) | Reference |
|----------|-----------------------------------|--|-------|-------------|----------|-------------------------|----------------------------|
| 10bzf | 55268.222 | 18 | D | 5.0 | 256 | < 33 | Chomiuk & Soderberg (2010) |
| " | 55337.221 | 87 | D | 6.0 | 1024 | < 36 | Corsi et al. (2011) |
| " | 55527.490 | 277 | C | 5.0 | 256 | < 35 | Corsi et al. (2011) |
| 10qts | 55426.028 | 13 | D | 8.5 | 256 | < 86 | Gal-Yam et al. (2010) |
| " | 55948.524 | 535 | DnC | 6.2 | 2048 | 39 | This paper |
| " | 55950.435 | 537 | DnC | 6.2 | 2048 | 28 | This paper |
| 10xem | 55767.647 | 297 | A | 5.0 | 256 | 66 | This paper |
| 10aavz | 55566.527 | 52 | C | 4.9 | 256 | 31 | Soderberg & Chomiuk (2011) |
| " | 55770.969 | 256 | A | 4.9 | 256 | 105 | This paper |
| 11cmh | 55692.145 | 19 | B | 8.4 | 256 | 45 | This paper |
| " | 55949.356 | 276 | DnC | 6.3 | 2048 | 159 ± 11 | This paper |
| " | 56766.099 | 1093 | A | 6.2 | 2048 | 17.4 ± 5.4 | This paper |
| " | 56781.411 | 1108 | " | 1.7 | " | 57 ± 13 | This paper |
| " | 56808.981 | 1136 | " | 2.9 | " | 18.0 ± 4.2 | This paper |
| 11img | 55781.981 | 31 | A | 5.0 | 256 | 48 | This paper |
| " | 55950.478 | 199 | DnC | 5.0 | 2048 | 66 | This paper |
| 11lbn | 55812.283 | 19 | A | 5.0 | 256 | 78 | This paper |
| " | 55948.043 | 155 | DnC | 6.2 | 2048 | 28 | This paper |
| 12as | 55933.555 | 8 | DnC | 6.2 | 2048 | 87 | This paper |
| " | 55947.382 | 22 | DnC | 6.2 | 2048 | 69 | This paper |
| " | 56999.567 | 1074 | C | 6.2 | 2048 | 75^{21} | This paper |
| 13u | 56391.376 | 67 | D | 6.2 | 2048 | 95^{22} | This paper |
| " | 56767.366 | 443 | A | 6.2 | 2048 | 14 | This paper |
| " | 57311.028 | 987 | D | 6.2 | 2048 | 100^{23} | This paper |
| 13alq | 56401.120 | 7 | D | 4.8 | 2048 | 30 | Kamble & Soderberg (2013) |
| 13alq | 56423.080 | 29 | DnC | 6.2 | 2048 | 60^{24} | This paper |
| 13alq | 57336.833 | 942 | D | 6.3 | 2048 | 33 | This paper |
| 13ebw | 56667.566 | 46 | B | 6.2 | 2048 | 15 | This paper |
| " | 57001.417 | 380 | C | 6.2 | 2048 | 41^{25} | This paper |
| 14dby | 56838.197 | 6 | D | 5.2 | 1024 | 33 | This paper |
| " | " | " | " | 7.5 | " | 40 ± 12 | " |
| " | 56853.994 | 22 | " | 5.2 | " | 40.1 ± 9.8 | " |
| " | " | " | " | 7.5 | " | 117 ± 12 | " |
| " | 56879.117 | 47 | " | 5.0 | " | 194 ± 12 | " |
| " | " | " | " | 7.4 | " | 279 ± 15 | " |
| " | 56889.108 | 57 | " | 2.5 | " | 164 ± 54 | " |
| " | " | " | " | 3.3 | " | 125 ± 18 | " |
| " | " | " | " | 8.5 | " | 176 ± 14 | " |
| " | " | " | " | 9.5 | " | 159 ± 14 | " |
| " | " | " | " | 13.5 | " | 107 ± 13 | " |
| " | " | " | " | 14.5 | " | 105 ± 13 | " |
| " | 56902.138 | 70 | " | 5.0 | " | 72 ± 19 | " |
| " | " | " | " | 7.4 | " | 73 ± 17 | " |
| " | 56903.045 | 71 | " | 2.7 | " | 121 ± 40 | " |
| " | " | " | " | 3.2 | " | 79 ± 16 | " |
| " | " | " | " | 8.5 | " | 108 ± 11 | " |
| " | " | " | " | 9.5 | " | 102 ± 11 | " |
| " | " | " | " | 13.5 | " | 56.5 ± 9.6 | " |
| " | " | " | " | 14.5 | " | 55.5 ± 9.7 | " |
| " | 56913.144 | 81 | " | 5.1 | " | 73 ± 18 | " |
| " | " | " | " | 7.5 | " | 60 ± 16 | " |
| " | 56914.770 | 83 | " | 8.5 | " | 61 ± 14 | " |
| " | " | " | " | 9.5 | " | 80 ± 15 | " |
| " | " | " | " | 13.5 | " | 38 ± 12 | " |
| " | " | " | " | 14.5 | " | 41 ± 13 | " |
| " | 56946.949 | 115 | DnC | 2.5 | " | 101 ± 28 | " |
| " | " | " | " | 3.5 | " | 138 ± 16 | " |
| " | " | " | " | 5.0 | " | 84 ± 12 | " |
| " | " | " | " | 6.0 | " | 79 ± 15 | " |
| " | " | " | " | 8.5 | " | 48 ± 10 | " |
| " | " | " | " | 9.5 | " | 59 ± 11 | " |
| " | 56998.800 | 167 | C | 2.5 | " | < 111 | " |
| " | " | " | " | 3.4 | " | 48 ± 13 | " |
| " | " | " | " | 5.0 | " | 53 ± 10 | " |
| " | " | " | " | 6.0 | " | 44 ± 14 | " |
| " | " | " | " | 8.5 | " | 28.9 ± 9.3 | " |
| " | " | " | " | 9.5 | " | 40 ± 11 | " |
| PTF14gaq | 56932.496 | 8 | DnC | 6.3 | 2048 | 28 | This paper |
| " | 56998.857 | 75 | C | 6.2 | 2048 | 25 | This paper |
| " | 57335.919 | 411 | D | 6.3 | 2048 | 19 | This paper |

²¹ 5σ UL corresponding to the brightness of the host galaxy.²² 10σ UL corresponding to the brightness of the host galaxy.²³ 10σ UL corresponding to the brightness of the host galaxy.²⁴ 3.6σ UL.²⁵ 7σ UL corresponding to the brightness of the host galaxy.

TABLE 3 VLA observations. For non-detections, the quoted UL are at 3σ (where σ is the image rms) unless otherwise stated.

| PTF Name | T_{VLA}^j (MJD) | ΔT_{VLA}^k (d) | Conf. | ν (GHz) | BW (MHz) | Flux (μJy) | Reference |
|----------|-----------------------------|----------------------------------|-------|----------------|-------------|----------------------------|------------|
| PTF15dld | 57336.049 | 18 | D | 5.0 | 2048 | $\lesssim 110^{26}$ | This paper |

^j The VLA observation time T_{VLA} is the time at the mid-point of the VLA observation.

^k VLA observation epoch in days since PTF discovery, not corrected for redshift effects.

²⁶ 10σ UL corresponding to the brightness of the host galaxy.